

July 2021

A Study of Methane-Liquid Absorption Characteristics for Gas Influx Management

Scott A. Perry

Louisiana State University and Agricultural and Mechanical College

Follow this and additional works at: https://digitalcommons.lsu.edu/gradschool_theses



Part of the [Other Engineering Commons](#)

Recommended Citation

Perry, Scott A., "A Study of Methane-Liquid Absorption Characteristics for Gas Influx Management" (2021).
LSU Master's Theses. 5419.

https://digitalcommons.lsu.edu/gradschool_theses/5419

This Thesis is brought to you for free and open access by the Graduate School at LSU Digital Commons. It has been accepted for inclusion in LSU Master's Theses by an authorized graduate school editor of LSU Digital Commons. For more information, please contact gradetd@lsu.edu.

A STUDY OF METHANE-LIQUID ABSORPTION CHARACTERISTICS FOR GAS INFLUX MANAGEMENT

A Thesis

Submitted to the Graduate Faculty of the
Louisiana State University and
Agricultural and Mechanical College
in partial fulfillment of the
requirements for the degree of
Master of Science

in

The Craft & Hawkins Department of Petroleum Engineering

by
Scott Allen Perry
B.S., University of Arkansas, 2019
August 2021

ACKNOWLEDGMENTS

I would like to first give a special thank you to my advisor, Dr. Yuanhang Chen, for allowing me this opportunity at Louisiana State University and his continued support and guidance throughout my graduate school studies, research and thesis development. Also, I would like to extend my sincere gratitude to my committee members, Dr. Mayank Tyagi and Dr. Seung Kam, for their time, advice and support during this process.

A special thank you goes to a fellow researcher, Damilola Ojedeji, as we started our time at LSU together, I could not have asked for a better friend to share advice and support with throughout our journeys. I would also like to thank my research group members, Shahriar Mahmud and James Nielsen, as they have been very helpful throughout this process.

Finally, I would like to thank several members of my family for the love and support they have shown. To my father and stepmother, Daniel and Michelle Perry, and mother and stepfather, Susan and Matthew Hicks, I could not be where I am today without the sacrifices, guidance and belief in me to accomplish my goals. To my sister, Caitlin, who has always been there for me through every situation. To all other family members who have supported me in my journey, I will be forever thankful for you.

TABLE OF CONTENTS

ACKNOWLEDGMENTS	ii
LIST OF TABLES.....	v
LIST OF FIGURES	vi
NOMENCLATURE	viii
ABSTRACT.....	x
Chapter 1. INTRODUCTION.....	1
1.1. Gas Influxes into Wellbore and Migration in Drilling Fluids.....	1
1.2. Applications of Mass Transfer Kinetics	3
1.3. Objectives of Thesis.....	6
Chapter 2. LITERATURE REVIEW.....	8
2.1. Methane Solubility in Non-Aqueous Drilling Fluids.....	8
2.2. Influence of Parameters on Mass Transfer Kinetics	10
2.3. Previous Studies of Absorption Mass Transfer Kinetics	19
2.4. Previous Studies of Interfacial Area	23
Chapter 3. EXPERIMENTAL DEVELOPMENT.....	27
3.1. Low Pressure Mass Transfer Apparatus	27
3.2. High Pressure Mass Transfer Apparatus.....	29
3.3. Material and Fluid Characterization	33
3.4. Volumetric Mass Transfer Coefficient Calculations	34
3.5. Image Analysis Calculations.....	37
3.6. Validation of Image Analysis Measurements	40
3.7. Experimental Design for Investigation of Parameters	43
Chapter 4. EXPERIMENTAL RESULTS.....	49
4.1. Solubility of Methane in Base Fluids.....	49
4.2. The Effect of Pressure, Superficial Gas Velocity and Fluid Type.....	50
4.3. The Effect of Sparger Design	52
4.4. The Effect of Column Diameter	53
4.5. The Effect of Elevated Pressure.....	54
Chapter 5. DATA ANALYSIS	56
5.1. Development of $k_L a$ Correlation	56
5.2. Image Analysis.....	58
Chapter 6. RECOMMENDATIONS AND CONCLUSION.....	64
APPENDIX A. Experimental Data Used for the Calculation of $k_L a$	66
APPENDIX B. Development of Dimensionless Mass Transfer Correlation	68

BIBLIOGRAPHY	70
VITA.....	74

LIST OF TABLES

2.1.	Parameters affecting absorption mass transfer coefficient	11
2.2.	List of literature studies of volumetric mass transfer coefficient in bubble columns	20
2.3.	List of literature studies of volumetric mass transfer coefficient correlations.....	20
2.4.	Previous literature studies using different techniques to calculate interfacial area	24
3.1.	Physical properties of diesel and internal olefin used in this study	34
3.2.	Experimental test matrix for the investigation of pressure, superficial gas velocity and fluid type	43
3.3.	Experimental test matrix for the investigation of sparger design	45
3.4.	Experimental test matrix for the investigation of column diameter	46
3.5.	Experimental test matrix for the investigation of elevated pressure.....	48
4.1.	Experimental results for the effect of sparger design on $k_L a$ values.....	52
5.1.	Experimental test matrix for $k_L a$ correlation.....	56
5.2.	Range of experimental conditions for developed $k_L a$ correlation.....	58
A.1.	Experimental data for absorption tests of methane in internal olefine at 100 psi and superficial gas velocities ranging from 0.45-2.51 cm/s	66
B.1.	Developed dimensionless mass transfer correlation for each pressure condition.....	69

LIST OF FIGURES

1.1.	Free gas absorption into uncontaminated drilling fluid	4
2.1.	Methane solubility at different temperature and pressures – Data from Feng et al. (2019)	9
2.2.	Influence of superficial gas velocity on mass transfer kinetics and interfacial area – Data from Jin et al. (2014)	12
2.3.	Influence of system pressure on $k_L a$ – Data from Jin et al. (2014)	13
2.4.	Influence of system pressure with an increase in superficial gas velocity on $k_L a$ – Data from Lau et al. (2004)	14
2.5.	Influence of operating temperature on $k_L a$ – Data from Jin et al. (2014)	15
2.6.	Influence of bubble column diameter on $k_L a$ – Data from Akita and Yoshida (1973)	16
2.7.	Dependency of flow regime on gas velocity and column diameter – Data from Shah et al. (1982)	17
2.8.	Influence of gas sparger opening on $k_L a$ – Data from Koide et al. (1984)	19
3.1.	PFD of the low-pressure mass transfer experimental lab apparatus	28
3.2.	High-pressure apparatus currently installed at the LSU PERTT Laboratory	31
3.3.	PFD of the high-pressure mass transfer experimental apparatus	32
3.4.	Total gas absorbed (L) of methane in internal olefin fluid at 100 psi and superficial gas velocities ranging from 0.45 to 2.51 cm/s	35
3.5.	Concentration of methane (mol/L) dissolved into internal olefin fluid over time at 100 psi and superficial gas velocities ranging from 0.45 to 2.51 cm/s	36
3.6.	Graph of $\ln\left(\frac{C^*}{C^*-C_L}\right)$ vs time (s) for the calculation of $k_L a$ for methane in internal olefin fluid at 100 psi and superficial gas velocities ranging from 0.45 to 2.51 cm/s	37
3.7.	Processed experimental images with increased superficial gas velocity	38
3.8.	Experimental images for ellipsoidal bubble calculation assumption	39
3.9.	Interfacial area in 20 second time intervals during the experimental test at 100 psi and 0.0090 m/s	41

3.10.	Images for interfacial area in 20 second time intervals at 100 psi and 0.0090 m/s	42
3.11.	Interfacial area values for assumption of spherical and ellipsoid bubbles.....	43
3.12.	Images of the sparger designs on the experimental apparatus.....	46
4.1.	The concentration of methane in diesel and internal olefines at complete saturation at a temperature of 295 K and various pressures ranging from 100 to 300 psi	50
4.2.	Experimental results for the effects of superficial gas velocity, system pressure and fluid type on $k_L a$ for methane absorption in non-aqueous fluids	51
4.3.	Experimental results for the effects of an increased range of superficial gas velocity (0.0045-0.049 m/s) and system pressure (100-300 psi) on $k_L a$ for methane absorption in nonaqueous fluids.....	52
4.4.	Experimental results for the effect of column diameter on $k_L a$ for methane absorption in non-aqueous fluids	54
4.5.	Experimental results for the effect of elevated pressure on $k_L a$ for methane absorption in non-aqueous fluids	55
5.1.	Experimental results for development of $k_L a$ correlation	57
5.2.	Image analysis results for the influence of superficial gas velocity on mass transfer kinetics and interfacial area	60
5.3.	Image analysis results for the influence of operating pressure on mass transfer kinetics and interfacial area	62
5.4.	Influence of superficial gas velocity and operating pressure on gas holdup	63

NOMENCLATURE

a	Interfacial Area [1/m]
C^*	Maximum gas concentration [mol/L]
C_f	Final concentration of gas in liquid [mol/L]
C_H	Concentration of a gas at a fixed temperature and pressure [M]
C_i	Initial concentration of gas in liquid [mol/L]
C_L	Concentration of gas in liquid [mol/L]
d_B	Individual bubble diameter [m]
d_S	Sauter mean bubble diameter [m]
D_c	Column diameter [cm]
D_H	Hydraulic equivalent diameter [m]
D_L	Diffusivity of solute gas into liquid [m ² /s]
D_o	Sparger diameter [mm]
$F_{emulsifier}$	Fraction of emulsifier in a blended fluid
F_{oil}	Fraction of oil in a blended fluid
F_{water}	Fraction of water in a blended fluid
g	Acceleration due to gravity [m/s ²]
H_c	Column height [m]
k_H	Henry's Constant [M/atm]
k_L	Liquid-side mass transfer coefficient [m/s]
$k_L a$	Volumetric mass transfer coefficient [1/s]
P	Pressure [psig]
R	Gas constant, $0.08205 \left[\frac{Latm}{Kmol} \right]$
R_s	Total solubility of a fluid [M]

$R_{s,oil}$	Solubility of the oil phase [M]
$R_{s,water}$	Solubility of the water phase [M]
$R_{s,emulsifier}$	Solubility of the emulsifier phase [M]
S	Surface area of ellipsoid bubble [m ²]
t	Time [s]
T	Temperature [K]
U_G	Superficial gas velocity [m/s]
U_{SL}	Superficial liquid velocity [m/s]
U_{SG}	Superficial gas velocity [m/s]
V_B	Volume of ellipsoid bubble [m ³]
V_C	Volume of liquid in the column [m ³]

Greek Symbols

ρ_G	Gas density [kg/m ³]
ε_G	Gas holdup
ν_L	Kinematic liquid viscosity [m ² /s]
ρ_L	Liquid density [kg/m ³]
σ	Liquid surface tension [dyne/cm]
μ_l	Liquid viscosity [Pas]

Unit Conversion

psi x 0.006895	=	MPa
inch x 0.0254	=	m
liters x 0.001	=	m ³

ABSTRACT

The study of absorption mass transfer kinetics in non-aqueous base fluids and the investigation of the parameters that influence this process is crucial in the application to gas influx management. While there have been a large number of studies investigating the interaction and solubility of methane in non-aqueous drilling fluids, relatively little attention has been placed on studying the mass transfer kinetics for different scenarios within the wellbore and riser. During the drilling process, there are multiple ways in which the formation gas can come into contact with the drilling fluid via a gas kick. Once the gas influx dissolves into the liquid and is circulated up the wellbore, the gas will come out of solution in the riser due to a decrease in pressure. During managed pressure drilling (MPD), the desorbed gas could potentially be redissolved back into the drilling fluid due to an increase in riser pressure from a MPD choke or backpressure pump manipulation. Absorption mass transfer can also be applied in other drilling or completion applications.

This study investigates several parameters that influence the absorption mass transfer kinetics experimentally, such as operating pressure, superficial gas velocity, fluid type, column diameter and sparger design are investigated. In the analysis of the results and supported by previous literature studies, superficial gas velocity and operating pressure have the most significant influence on the volumetric mass transfer coefficient ($k_L a$). As a result, a correlation has been developed under the ranges of operating conditions for $k_L a$ as a function of superficial gas velocity and operating pressure. Following the development of the correlation, an image analysis of the experiments was conducted to separate the $k_L a$ values into the liquid-side mass transfer coefficient (k_L) and interfacial area (a). This study is expected to help future applications of gas influx management and well control events.

Chapter 1. INTRODUCTION

1.1. Gas Influxes into Wellbore and Migration in Drilling Fluids

The study of drilling fluids started in the 1980s, when researchers began to focus on the interaction between formation gas and the fluids that were used in the drilling and completion processes. The understanding of this interaction between gas and fluids at high bottom hole pressures is crucial to safely handle well control events. Oil based drilling fluids (OBDF) have been the most used and preferred fluids for deep-water wells. They have several beneficial properties compared to water-based fluids like better lubrication, reduced formation damage, better borehole stability and high-pressure high-temperature (HPHT) tolerance (Skogestad et al. 2017). Despite the added benefits of OBDF, there are several potential problems associated with formation gas.

There are multiple ways for the formation gas to come into contact with the drilling fluid causing the drilling fluid to become contaminated. The first, is when the circulated drilling fluid at bottomhole pressures is at a lower pressure than the formation that is being drilled through. Because of the pressure difference, the gas in the formation enters the wellbore which is known commonly as a “gas kick”. When a water-based drilling fluid is used, the formation gas is not very soluble in the water-based fluid leading to a pit gain at the surface equal to the volume of formation gas at the bottom hole pressure and temperature conditions. However, when an oil-based drilling fluid is used, the formation gas is much more soluble in the oil-based fluid. Because the solubility is much higher, the gas can dissolve into the fluid quickly and go undetected at the surface without any initial pit gain (O’Bryan et al. 1988).

Other methods of gas entering the wellbore and contaminating the drilling fluid is by drilled gas or gas entering the wellbore in a static well. Unlike an influx of gas with insufficient bottomhole pressure, drilled gas enters the wellbore when the formation that contains gas is drilled through. The pore spaces in the formation contains gas and that formation gas will migrate up the wellbore with the cuttings and mix with the drilling fluid. Like an under-pressured gas kick, the detectability of drilled gas depends on the fluid type used in the process. Formation gas can also enter the wellbore when the well is static and the drilling fluid is not being circulated. Bradley et al. (2002) suggested that several cubic meters of methane can diffuse into OBDF during a static well environment, even if the well is overbalanced. In this study, it reported that in a static 1000-meter HPHT horizontal well, the rate of methane diffusing into the OBDF could be 2.9 m³ of formation gas in the first 24 hours. If the well is not being used for an extended period of time during drilling or completion processes, it was reported that 18 m³ of gas could be absorbed into the fluid if left static for 50 days.

Gas solubility, particularly methane in various base oils, in a range of pressure and temperatures has been the focus of several research studies (O'bryan et al. 1988, Silva et al. 2004, Ribeiro et al. 2006, Linga et al. 2017). All these studies have been used to address gas loading characteristics and the impact that it has during well control events. Several methane solubility measurements have been made and are accurately modelled at pressures below the critical point. Further experimental work by Flatabø et al. 2015 expands the research from gas solubility in oil-based fluids. This study investigated density and viscosity values for methane saturate in base oils at pressures and temperatures similar to operating conditions (Flatabø et al. 2015). These calculations led to more accurate methane solubility values in drilling fluids and correct calculation of bottom hole pressure for HPHT operation conditions. O'bryan et al. (1988) discussed methane

solubility in both water-based and oil-based drilling fluids and considered the effect for well control problems. According to this study, the solubility of methane in oil-based fluids can be up to 100 times greater than the solubility in water-based fluids. This leads to severe problems in handling well control events when an influx of gas is taken during drilling with oil-based fluids. A study by Silva et al. (2004) looked at gas solubility in synthetic fluids to safely drill deep and ultradeep water wells economically. Overall, the better understanding of gas solubility in synthetic and oil-based fluids, will play a crucial role in terms of prevention, better gas kick detection and corrective well control practices when circulating a kick out of the hole.

1.2. Applications of Mass Transfer Kinetics

A unique scenario of gas absorption in well control operations is when dissolved or free gas passes the subsea blowout preventer (SSBOP), enters the riser, and begins to evolve from solution. Figure 1.1 shows that as free gas migrates to the surface, the free gas could be absorbed into the uncontaminated drilling mud due to the slippage between the gas and liquid phase during riser gas handling. With new drilling techniques and technologies, like managed pressure drilling, riser gas migration can be better controlled and managed because of their ability to quickly change the equivalent circulating density (ECD) of the fluid within the well. During MPD, a choke can be used at the surface to adjust the flow rate of drilling fluid and subsequently increase the pressure within the riser. Once the pressure is increased using the MPD choke or a backpressure pump, the expansion of free gas that has desorbed from the drilling fluid could potentially be absorbed back into solution when the gas slippage exposes the free gas to uncontaminated drilling fluid (Malloy et al. 2009). It is important to understand the behavior of gas absorption with different types of drilling fluids to control and prevent significant problems during well control in such events.

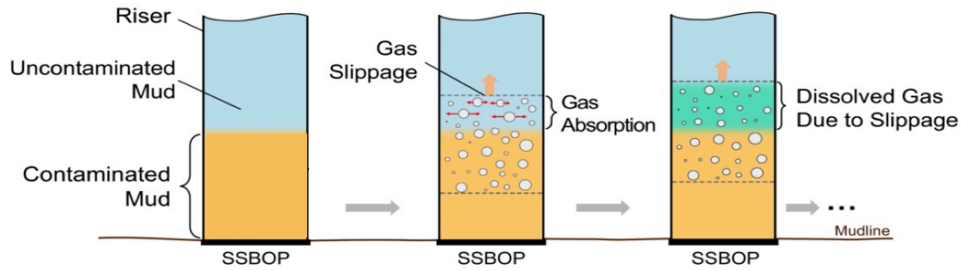


Figure 1.1. Free gas absorption into uncontaminated drilling fluid

It is crucial to understand and evaluate the process of gas absorption as a time-dependent process instead of an instantaneous equilibrium process for a few key reasons. As mentioned before, free gas from contaminated mud will come into contact with uncontaminated mud in the riser due to gas slippage. First, if absorption is considered an instantaneous process, it would result in the conclusion that any volume of mud contacting the gas phase becomes saturated immediately. Second, if gas absorption is considered in the radial direction only, free gas would dissolve into the mud surrounding it instantaneously while gas slippage occurs leading to an unrealistic scenario that all the fluid behind the front of the free gas would be completely saturated. Lastly, assuming gas absorption in all directions results in an unrealistic scenario that the free gas would dissolve into the entire mud column instantaneously, making it impossible for the free gas to exist or migrate in the riser in most scenarios. Therefore, assuming instantaneous absorption is unrealistic and could lead to large errors in simulation results which indicates the importance and necessity of considering absorption as a time-dependent process.

Another scenario in which gas absorption and mass transfer kinetics can be of importance is in sustained casing pressure (SCP) buildup and surface casing vent flow (SCVF) when leaked gas comes into contact with annular liquid above the cement in an open or closed annulus. Sustained casing pressure is a common occurrence with in 11,000 casing strings and over 8,000

wells (Bourgoyne et al. 1999). With SCP buildup, there is a primary concern that a down-hole situation could cause an underground blowout if not handled properly. In SCP buildup, the flow of gas through the vertical column of annular liquid has a low gas flow rate resulting in a likely bubbly flow regime. The porous cement acts as a bundle of orifices and allows gas bubbles to continuously form and flow up the annulus (Xu et al. 2002). In most scenarios, SCP buildup starts after a delay in time due to an absorption of leaked gas into the annular liquid. If gas absorption and mass transfer rates are not considered, the SCP buildup would start immediately without a delay (Lackey et al. 2019). Depending on the magnitude of the mass transfer rate, the solubility of methane in the liquid column could be reached quickly or could allow the gas to escape before the solubility limit was reached in surface casing vent flow. This is another key scenario in which the absorption mass transfer kinetics of methane in drilling or completion fluids is important to handle well control events.

As several studies have investigated the solubility of methane in nonaqueous fluids, the mass transfer kinetics of gas influxes need to be investigated for gas influx management events. Currently, there are several unknowns with gas absorption due to gas influxes and most industrial simulators still consider absorption as an instantaneous process instead of a time dependent process. This study investigates the influence of operating pressure and superficial gas velocity on the overall volumetric mass transfer coefficient ($k_L a$), liquid-side mass transfer coefficient (k_L), interfacial area (a), and gas holdup using experimental tests and image analysis. Absorption mass transfer kinetics has been studied for decades and the volumetric mass transfer coefficient has been determined for several different applications. Equations 1.1-1.3 show the model proposed by Alvarez et al. (2000) to calculate $k_L a$ values for mass transfer absorption experiments:

$$\frac{dC}{dt} = k_L a * (C^* - C) \quad [1.1]$$

$$\ln\left(\frac{C^*}{C^* - C_L}\right) = k_L a * t \quad [1.2]$$

$$k_L a = \frac{1}{t} * \ln\left(\frac{C^*}{C^* - C_L}\right) \quad [1.3]$$

In the study by Alvarez et al. (2000), experiments with CO₂ and an aqueous solution of sucrose and surfactants in a bubble column were performed to determine $k_L a$. Similarly, the same model used in the CO₂ experiments and several other literature studies of the volumetric mass transfer coefficient can be applied to describe mass transfer in absorption with methane and non-aqueous base fluids.

1.3. Objectives of Thesis

The results of the study of mass transfer absorption kinetics of gas influxes into non-aqueous drilling fluids can lead to a better understanding of the absorption process and provide important information for simulations of gas migration behaviors during a riser gas handling event. The absorption coefficient is impacted by 13 parameters (Ghandi et al. 2009), among which several parameters are investigated in this study such as system pressure, superficial gas velocity, fluid type, column dimensions, and sparger design. The primary goal is to develop a methodology and experimental design that accurately represents the absorption process in well control events, to better understand the absorption mass transfer in different scenarios of riser gas management.

This study is divided into three experimental sections as well as an extensive literature review understanding the process of gas absorption. The first section investigates system pressure, superficial gas velocity and liquid type with a low pressure experimental apparatus to determine the feasibility of this project. Once the effects on the absorption coefficient are determined at low

pressures, similar experiments were performed at high pressures similar to the environment during a well control event as the second section. The last section investigates other parameters like column dimensions and sparger design to make it possible to scale up the results to industrial well control scenarios. Following the experimental parametric study, image analysis is performed to separate the $k_L a$ into k_L and a to evaluate the influence of certain parameters on these values separately. Along with image analysis, a correlation is developed for the absorption mass transfer coefficient as a function of superficial gas velocity and operating pressure. The experimental results, image analysis and new correlation provided by this study allows for future simulation work using models to predict the behavior of gas influxes and gas migration for enhanced well control.

Chapter 2. Literature Review

2.1. Methane Solubility in Non-Aqueous Drilling Fluids

The investigation of gas solubility for methane in non-aqueous drilling fluids has been the focus of several previous research studies at various pressure and temperature ranges (O'bryan et al. 1988, Silva et al. 2004, Ribeiro et al. 2006, Linga et al. 2017). O'bryan et al. (1988) focused on the study of methane solubility in both water-based and oil-based drilling fluids and described the impact of methane solubility in well control events. The governing equation for the relationship between gas solubility and partial pressure is Henry's Law, which is shown in Equation 2.1.

$$C_H = k_H P_{gas} \quad [2.1]$$

Where C_H is the concentration of dissolved gas, k_H is Henry's Law constant and P_{gas} is the partial pressure of the gas.

The concentration of the gas in the liquid at complete saturation is a function of the partial pressure and the temperature of the system. If there is a change in the system, the increase or decrease in pressure shifts the equilibrium and there will be a change in solubility of a gas in a particular liquid. The solubility of a gas in a nonaqueous drilling fluid can be estimated by the following equation:

$$R_{sm} = R_{s,oil}F_{oil} + R_{s,water}F_{water} + R_{s,emulsifier}F_{emulsifier} \quad [2.2]$$

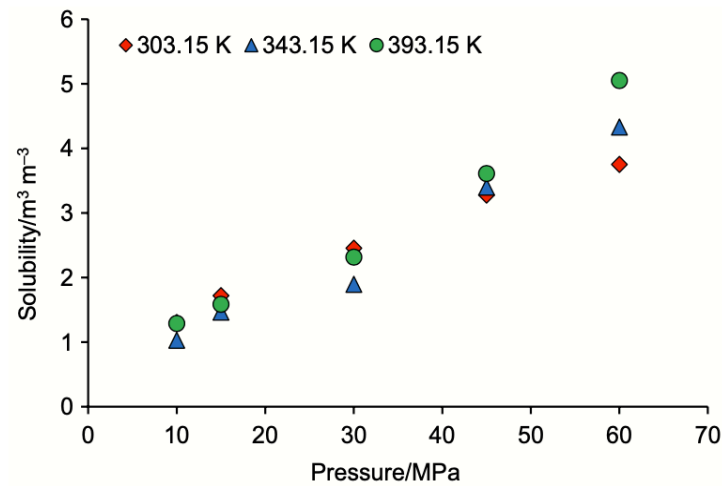
Where R_s is the solubility of the mixture and each phase and F is the fraction of each phase in the mixture.

O'bryan et al. (1988) presented an empirical equation for predicting the solubility of methane, ethane, and carbon dioxide in base oil and is shown in Equation 2.3:

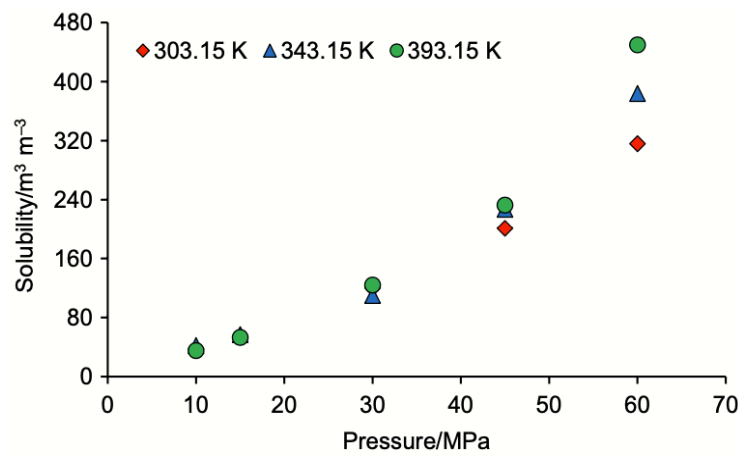
$$R_{so} = \left[\frac{P}{aT^b} + c \right]^n \quad [2.3]$$

In the empirical equation, R_{so} is the gas solubility in base oil in SCF/STB, at constant pressure (psia) and temperature ($^{\circ}\text{F}$) values and with constants a , b , c , and n determined for different types of gas-liquid systems.

Methane solubility in water-based and oil-based muds was experimental determined at different pressure and temperatures by Feng et al. (2019) and is shown in Figure 2.1.



(a)



(b)

Figure 2.1. Methane solubility at different temperatures and pressures – Data from Feng et al. (2019) (a) Methane solubility in water-based mud (b) Methane solubility in oil-based mud.

From the experimental results from Figure 2.1, it shows that gas solubility in oil-based mud is 10-100 times the solubility in water-based mud. As pressure increases, there is an increase in the solubility increment, where at first there is a linear trend between pressure and solubility before it becomes exponential at higher pressures. As the pressure increases the temperature has more of an influence on solubility at higher pressures compared to the temperature effect at lower pressures. With various non-aqueous fluids being used in drilling operations, the solubility under operating conditions is important to understand the interaction between formation gas and drilling fluids.

With methane dissolution in mud, phase equilibrium theory is used to study this process as it is a vapor-liquid equilibrium behavior (Feng et al. 2019). When the vapor-liquid mixture is at equilibrium, the chemical potential and fugacity of each component are equal in the vapor and liquid phases. To better understand the thermophysical properties of the mixture of methane and drilling fluids, binary interaction parameters (BIPs) need to be determined between those two components. Further modeling work using various equations of states could be used to better model the phase equilibrium of methane and oil-based mud binary systems. Based on developed models for phase equilibrium, leads to better understanding of the annulus flow behavior of gas during deepwater kick scenarios (Feng et al. 2019).

2.2. Influence of Parameters on Mass Transfer Kinetics

There are several key factors that can affect the absorption mass transfer coefficient. Table 2.1 shows all the 13 key parameters affecting gas-liquid mass transfer provided by Ghandi et al. (2009). Out of the 13 parameters, this experimental study investigated the effects of superficial gas velocity, system pressure, fluid type and sparger type on the volumetric mass transfer coefficient.

Although not all 13 parameters were investigated in this study, they have been investigated in previous experimental studies.

Table 2.1. Parameters affecting absorption mass transfer coefficient

Key Parameters Affecting Absorption Mass Transfer Coefficient	
Column Dimensions	Diameter Height
Sparger Type	Hole Diameter (Bubble Diameter) Number of Holes
System Properties	Temperature Pressure
Superficial Velocity	Gas Liquid
Liquid Properties	Density Viscosity Surface Tension
Gas Properties	Density Viscosity

2.2.1. Influence of Superficial Gas Velocity

One of the most investigated parameters in previous mass transfer experiments is the effect of superficial gas velocity (U_{SG}) on the volumetric mass transfer coefficient (Alvarez et al. 2000; Lau et al 2004; Jin et al. 2014). The superficial gas velocity has a crucial influence on operations of bubble and slurry bubble columns and in the case of this studies application, has a significant impact in offshore risers and wellbores. Increases in $k_L a$ values due to increased gas velocities, shown in Figure 2.2, come mostly from an increase in interfacial area. There is a higher interfacial area at high gas velocities because the average bubble size decreases up to a certain point due to bubble breakup. With an increase in the number of smaller bubbles, there is also a significant increase in gas holdup within the system (Lau et al. 2004). Along with an increase in $k_L a$ and

interfacial area, there is an increase in the liquid side mass transfer coefficient (k_L) due to an increase in turbulence created by the higher gas velocities. Although there is a reduction in contact time between the liquid and gas at higher gas velocities, the increase in interfacial area and k_L is still significant enough to cause an increase in the $k_L a$ values.

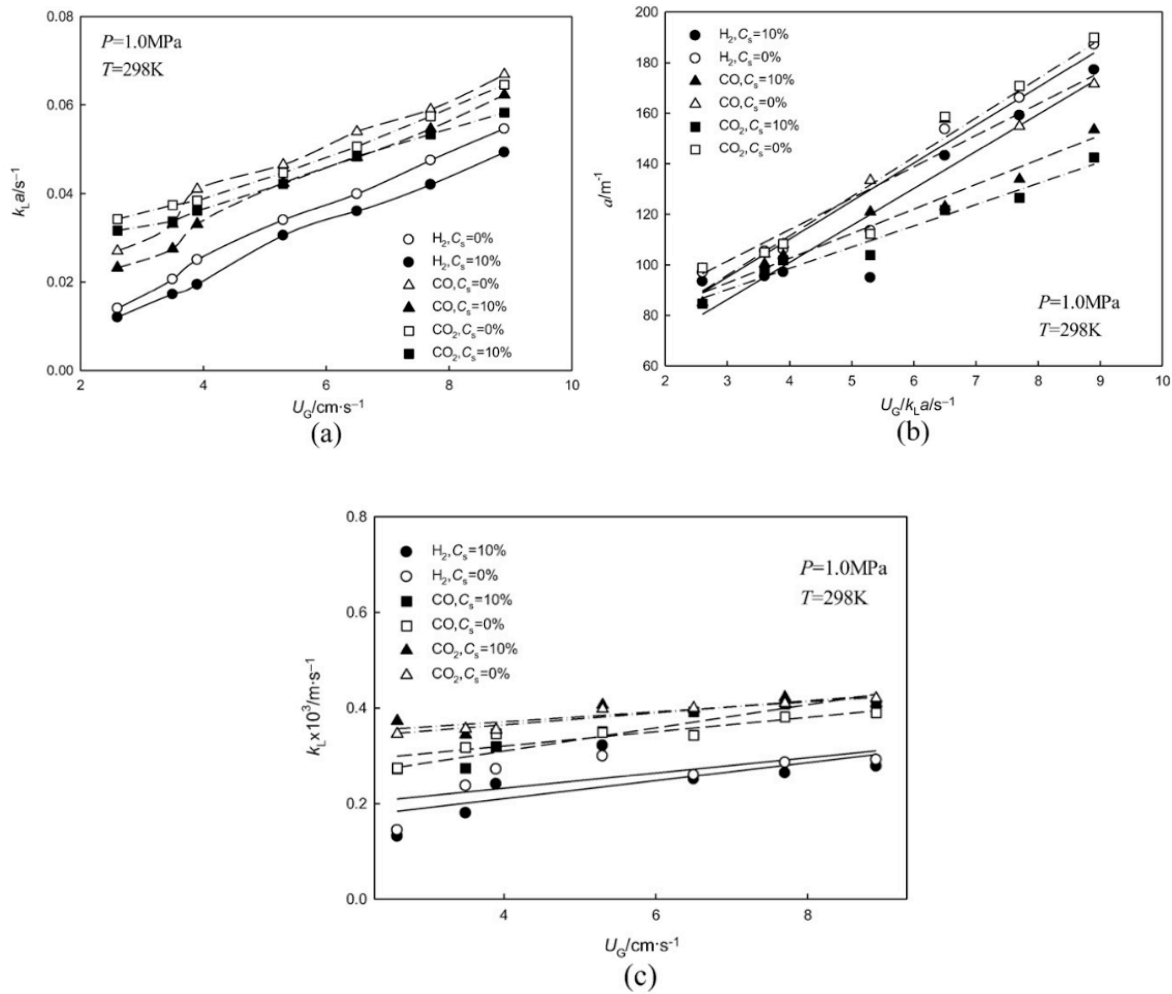


Figure 2.2. Influence of superficial gas velocity on mass transfer kinetics and interfacial area – Data from Jin et al. (2014) (a): Influence of U_{SG} on $k_L a$. (b): Influence of U_{SG} on a . (c): Influence of U_{SG} on k_L .

2.2.2. Influence of Pressure

Unlike with an increase in superficial gas velocity, where there was an increase in k_L and interfacial area, an increase in system pressure results in an increase in the $k_L a$ values because of an increase in interfacial area. As system pressure increases, bubble size decreases due to bubble breakup from higher gas density. As bubbles collapse, the bubble's size becomes smaller. The interfacial area will then increase between liquid and gas significantly resulting in an increase of $k_L a$ at higher pressures, as shown in Figure 2.3.

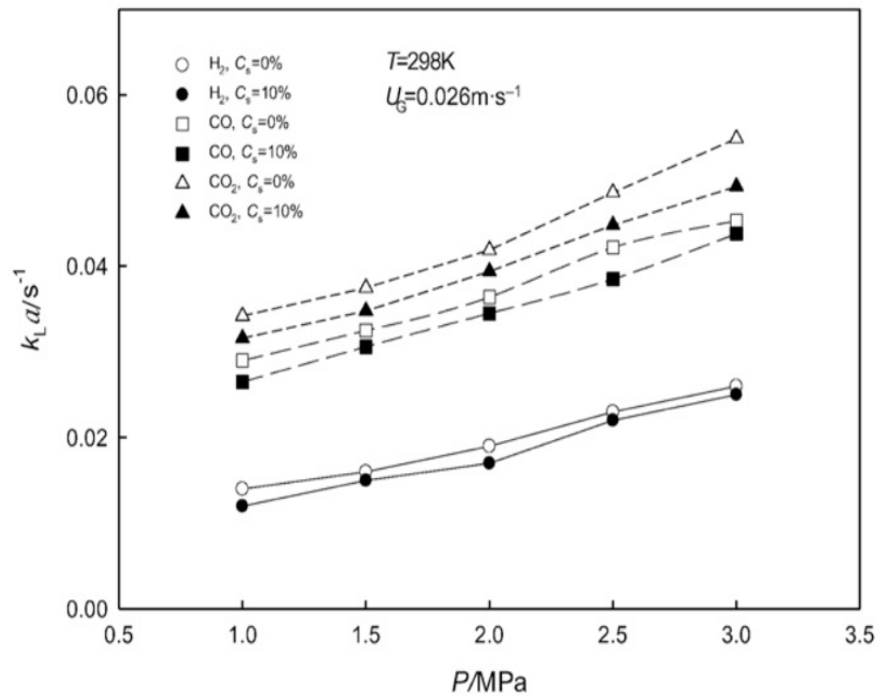


Figure 2.3. Influence of system pressure on $k_L a$ – Data from Jin et al. (2014)

At higher superficial gas velocities, the effect of pressure becomes even more noticeable. Figure 2.4 shows that pressure does not have as significant of an impact at lower superficial gas velocities, but once the superficial gas velocity is increased there is a more apparent impact on the $k_L a$ values.

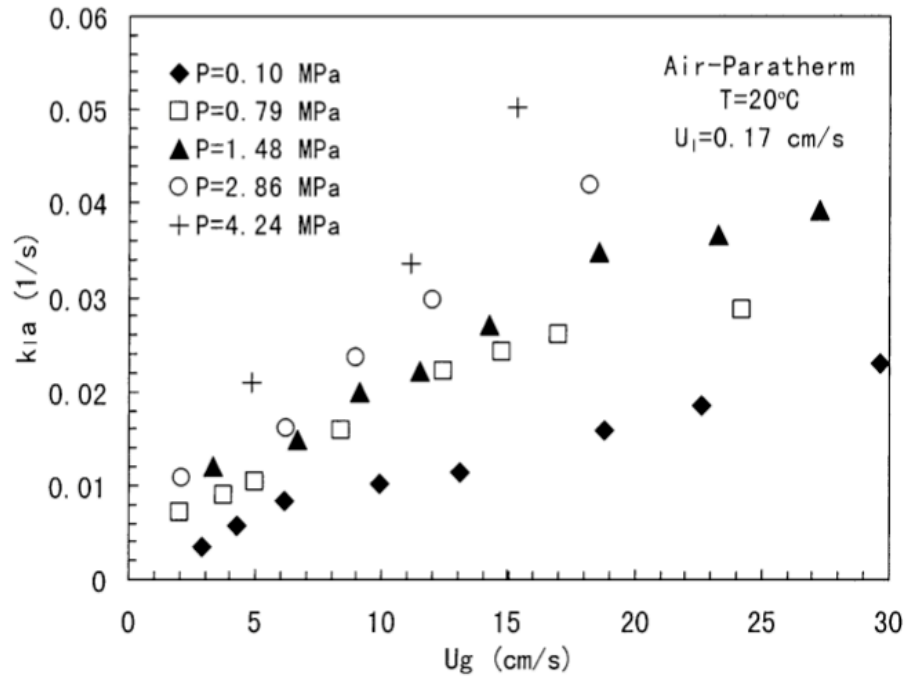


Figure 2.4. Influence of system pressure with an increase in superficial gas velocity on $k_L a$ – Data from Lau et al. (2004)

2.2.3. Influence of Temperature

Jin et al. (2014) also investigated the influence of operating temperature on mass transfer kinetics with CO, CO₂ and H₂ and the results are shown in Figure 2.5. The experimental study showed that $k_L a$ increases with increasing temperature. The gas diffuse coefficient and liquid properties, surface tension and viscosity, were strongly affected by the increase in temperature resulting in an impact on the $k_L a$ values. With an increase in operating temperature, there was a decrease in liquid-gas surface tension and liquid viscosity. This led to the ability for the formation of smaller gas bubbles leading to an increase in the interfacial area, gas holdup and volumetric mass transfer coefficient (Jin et al. 2014). Although the decrease in liquid viscosity will lead to higher bubble rising velocity and shorter contact time, the increase in interfacial area has more influence on the increase in $k_L a$ values.

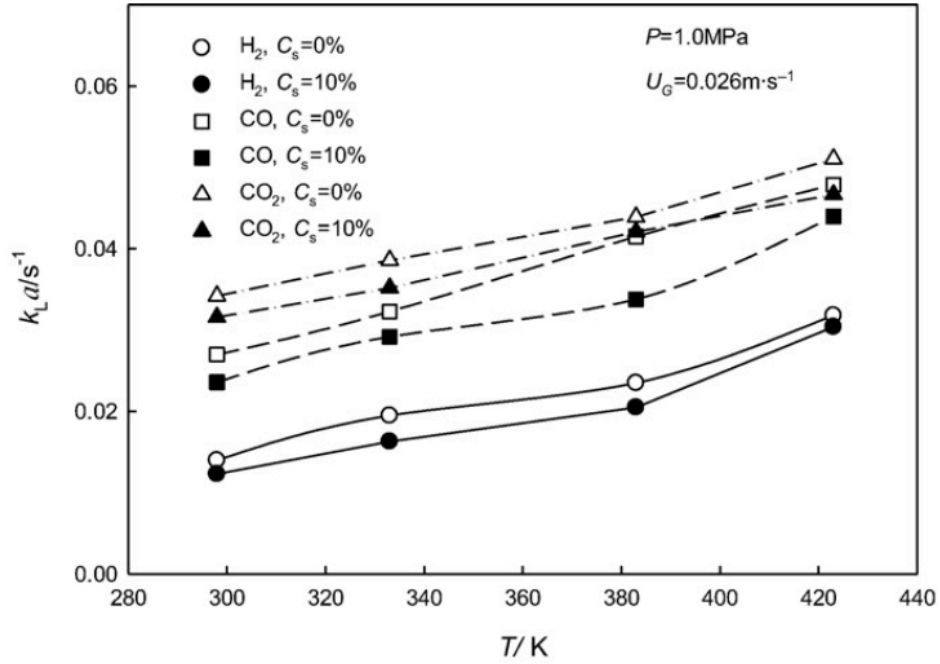


Figure 2.5. Influence of operating temperature on $k_L a$ – Data from Jin et al. (2014)

2.2.4. Influence of Column Diameter

From Akita and Yoshida (1973), the $k_L a$ values are related to bubble column diameter up to a diameter of 0.15 meters and the experimental results are shown in Figure 2.6. Columns larger than 0.15 meters are considered larger diameter bubble columns and they have no influence on the mass transfer coefficient. Along with the column diameter, the aspect ratio (AR), liquid height over column diameter (H/D_c), influences the $k_L a$ values. In bubble columns with an $AR < 5$, the flow patterns and regimes are not completely developed causing the aspect ratio and sparger type to have larger influence on the mass transfer rate.

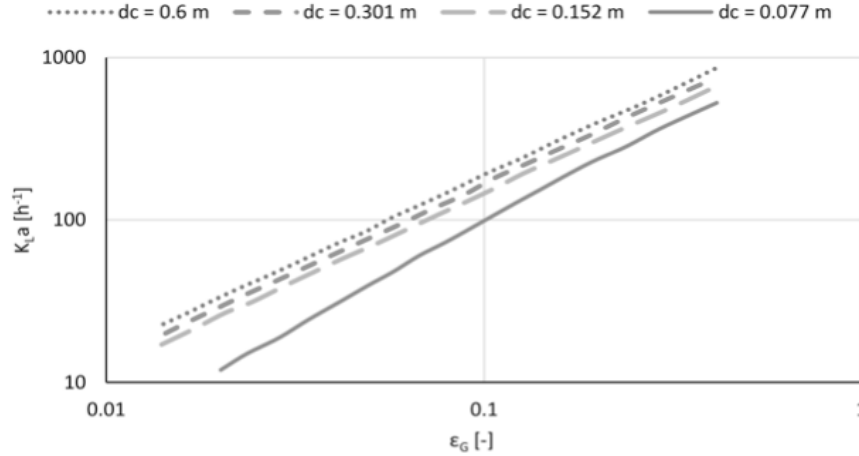


Figure 2.6. Influence of bubble column diameter on $k_L a$ – Data from Akita and Yoshida (1973)

According to Wilkinson et al. (1992), there are three main criteria for scaling up mass transfer coefficient results and to remove the influence of bubble column dimensions when scaling up from a laboratory scale to a larger industrial scale bubble column. The same can be true in this study when scaling up $k_L a$ values from laboratory mass transfer absorption experiments to be used in simulation work for well control events. The three main criteria are as follows:

1. A bubble column diameter, $D_c > 0.2$ meters, which ensures that the experimental results come from a bubble column that is not operating at slug flow conditions. This ensures that when scaling up to an offshore riser, that the lab scale experimental results match the gas flow conditions of the larger columns flow regime. This criterion agrees with the large diameter concept and experimental results discussed earlier in this section.
2. Aspect ratio (AR) is greater than 5. This ensures that liquid height does not influence the results by having a large enough liquid height compared to the column diameter.
3. Sparger diameter should be greater than 2 mm. With the sparger classified as a coarse bubble distributor, a significant change in the superficial gas velocity will not change the flow regime allowing the hydrodynamics and mass transfer rates to be insensitive to the

sparger design. With a fine bubble diffuser (sparger diameter < 2.0 mm), the flow regime will change with an increase in superficial gas velocity making it difficult to scale up resulting $k_L a$ values.

The mass transfer experimental apparatus used in this study meet both criteria 2 and criteria 3. The lack of practicality of criteria 1 in a laboratory is addressed by Deshpande et al. (2019). To justify the scaling up of results in a bubble column with a $D_c < 0.2$ meters, the criteria of not obtaining results from the slug flow regime must be met. By ensuring the experiments are carried out in a bubbly flow or heterogenous churn regime, instead of the slug flow regime, allows for the mass transfer rates not to be influenced by the smaller column dimensions and justifies the use of the more practical laboratory scale apparatus. In this study, experiments on the experimental apparatus, $D_c = 0.0254$ meters, are performed at superficial gas velocities, $U_G < 0.05$ m/s, which prevents experiments from being conducted in the slug flow regime according to Figure 2.7 from Shah et al. (1982).

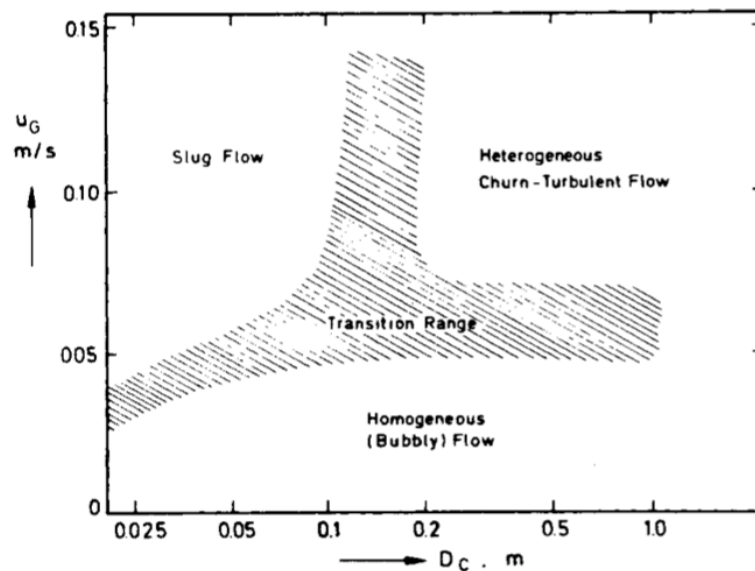


Figure 2.7. Dependency of flow regime on gas velocity and column diameter – Data from Shah et al. 1982

2.2.5. Influence of Sparger Design

Certain gas sparger openings and sparger designs have a large influence on the two-phase hydrodynamics. When designing a sparger to improve the efficiency of mass transfer in industrial practices, a fine bubble diffuser or porous plate should be used to decrease average bubble diameter and increase the interfacial area. With a fine sparger ($D_o < 2.0$ mm), at low enough superficial gas velocities, the velocity can generate a homogenous flow regime and transition into a heterogeneous regime when the gas velocity is increased. This transition in flow regime makes it difficult to predict $k_L a$ values and scale up results to larger bubble columns as the sparger has a significant influence over the mass transfer kinetics.

Because of the lack of control with a fine bubble sparger, a coarse bubble sparger ($D_o > 2.0$ mm) is preferred in this experimental study to remove the effect of sparger design on the mass transfer coefficient. With the coarse bubble sparger, the flow regime is always in the heterogeneous flow regime even at low superficial gas velocities, meaning there is no transition in flow regime with an increase in velocity. Because the flow regime is consistent with the coarse bubble sparger, the resulting hydrodynamics and mass transfer rates are insensitive to sparger design (Deshpande et al. 2019). This understanding of the effect of sparger orifice diameter is investigated further in this experimental study and satisfies criteria number 3 from Wilkinson et al. (1992) in the three criteria needed to upscale bubble columns from laboratory scale to industrial applications.

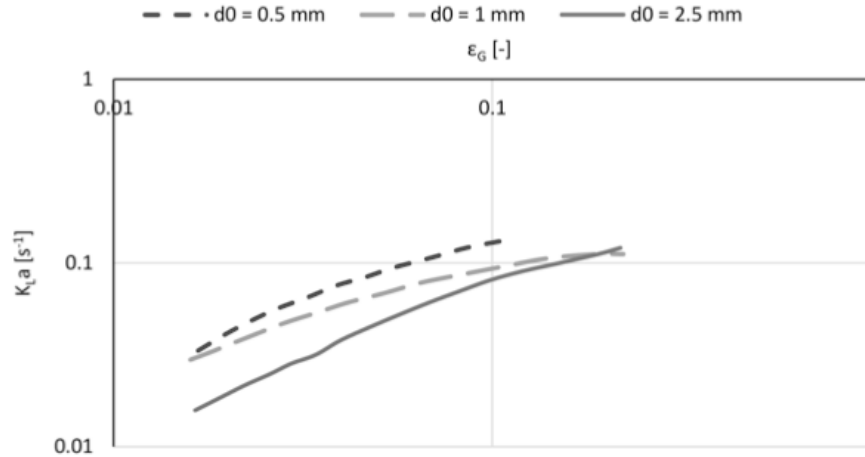


Figure 2.8. Influence of gas sparger opening on $k_L a$ – Data from Koide et al. (1984)

Figure 2.8 shows the influence of gas sparger openings on the resulting $k_L a$ values. $k_L a$ increases significantly with a decrease in sparger diameter (D_o) and increases with an increase in gas holdup. Once a coarse bubble sparger is used, the further enhancement of gas holdup and mass transfer rates in the heterogeneous flow regime with an increase superficial gas velocity is minimal. When using the gas sparger ($D_o > 2.0$ mm) the gas sparger opening no longer has an influence on the $k_L a$ values and allows for scaling up the mass transfer coefficients.

2.3. Previous Studies of Absorption Mass Transfer Kinetics

Table 2.2 provides a list of previous experimental studies in literature that investigates the effect of various parameters on the volumetric mass transfer coefficient in bubble columns. Due to limitations in this study, the effects of certain parameters can only be analyzed by previous studies found in literature. While this experimental study investigates superficial gas velocity, system pressure, fluid type, column diameter and sparger design, it is important to analyze the effect of parameters like system temperature, liquid properties and gas properties when developing a volumetric mass transfer correlation. These previous literature studies have been reviewed

because of the investigation of additional parameters that are not investigated in this study and are further discussed throughout this study.

Table 2.2. List of literature studies of volumetric mass transfer coefficient in bubble columns

<i>Authors</i>	<i>Experimental Setup</i>	<i>Gas-Liquid System</i>	<i>Purpose</i>
<i>Alvarez et al.</i>	Bubble Column	CO ₂ – SLS – Sucrose	Study the effect of σ , μ , ρ , U_G , and porous size on k_La
<i>Jin et al.</i>	Bubble Column	H ₂ , CO, CO ₂ – Liquid Paraffin	Study the effect of T, P, U_G , and slurry concentration on k_La , k_L and a
<i>Lau et al.</i>	Bubble Column	Nitrogen, Air – Water/Paratherm NF Fluid	Study the effect of P, T, U_G , U_L , liquid properties, and column dimensions on k_La
<i>Deckwer et al.</i>	Multiple Bubble Columns	Oxygen – Tap Water/Salt Solutions/Molasses	Develop k_La correlation dependent on U_G with multi hole sparger
<i>Shah et al.</i>	Multiple Bubble Columns	Oxygen – Tap Water/Salt Solutions	k_La correlations based on U_G with different sparger designs
<i>Hikita et al.</i>	Multiple Bubble Columns	Air – Water/Electrolyte Solutions	k_La correlation based on U_G with a single-nozzle coarse sparger
<i>Kojima et al.</i>	Bubble Column	N ₂ , O ₂ – Tap Water, Aqueous Solution of Enzyme	Study the effect of U_G , P and Sparger diameter on k_La

Mass Transfer Kinetics Correlations

Table 2.3. List of literature studies of volumetric mass transfer coefficient correlations

<i>Authors</i>	<i>k_La Values (s⁻¹)</i>	<i>Range of Parameters</i>	<i>k_La Correlation</i>
<i>Alvarez et al.</i>	(1.1-2.2) x 10 ⁻³	$U_{SG} = 0.0007-0.0016$ m/s $\sigma = (65-72) \times 10^3$ N/m $\mu = (0.9-1.15) \times 10^3$ $D_o = 0.06-0.18$ mm	$k_La = k_i U_{SG}^{2/3} \sigma^{3/4} \mu^{-3/4} \rho^{3/2}$
<i>Jin et al.</i>	(1-8) x 10 ⁻²	$U_{SG} = 0.03-0.10$ m/s P = 1-3 MPa, T = 298-423 K C_s (quartz sand) = 0-20%	$k_La = 3.051 \times (\rho_L v_A / M_B)^{-1.193} Sc^{-0.734} (\rho_G U_{SG})^{0.524} (1 - C_s / 0.85)^{2.303}$

(table cont'd.)

Authors	$k_L a$ Values (s^{-1})	Range of Parameters	$k_L a$ Correlation
<i>Lau et al.</i>	$(0.1-25) \times 10^{-2}$	$D_c = 0.045-0.45$ m $U_{SG} = 0.01-0.6$ m/s $P = 0.1-4.24$ MPa $\sigma = 0.023-0.073$ N/m	$k_L a = 1.77\sigma^{-0.22}e^{1.65U_L-65.3\mu_L\epsilon_g^{1.2}}$
<i>Deckwer et al.</i>	$(0.5-20) \times 10^{-2}$	$D_c = 0.2$ m, $H_c > 1$ m, $U_{SG} = 0.004-0.01$ m/s Multi-hole sparger $D_o = 1$ mm	$k_L a = \alpha U_{SG}^\beta$ $\alpha=0.49$ $\beta=0.88$
<i>Shah et al.</i>	$(0.5-20) \times 10^{-2}$	$D_c = 0.15-0.2$ m, $H_c > 2-7$ m, $U_{SG} = 0.002-0.08$ m/s Multi-hole sparger $D_o = 1$ mm Fine Sparger $D_o = 0.15$ mm	$k_L a = \alpha U_{SG}^\beta$ Multi-hole: $\alpha=0.47$ $\beta=0.82$ Fine Sparger: $\alpha=1.17$ $\beta=0.82$
<i>Hikita et al.</i>	$(1-20) \times 10^{-2}$	$D_c = 0.1-0.19$ m, $H_c = 2.2$ m, $U_{SG} > 0.04$ m/s Single Hole Sparger $D_o = 10$ mm	$k_L a = \alpha U_{SG}^\beta$ $\alpha=0.61$ $\beta=0.76$
<i>Kojima et al.</i>	$(1-6) \times 10^{-2}$	$D_c = 0.045$ m, $H_c = 0.9-1.2$ m, $U_{SG} = 0.005-0.15$ m/s, $P = 0.1-1.1$ MPa	$k_L a = C\epsilon_G^D(\rho Q^2 d_o^{-3}\sigma^{-1})^E \left(\frac{P}{P_0}\right)^F$

Table 2.3 shows some of the literature studies to this point that provide the results on the effect of parameters and the developed empirical correlations for the volumetric mass transfer coefficient that describe the various experiments presented. Because of the complexity of the hydrodynamic conditions encountered, several different types of volumetric mass transfer correlations were developed based on different parameters with very specific and narrow operating conditions. The estimation of $k_L a$ has been a topic of research for several years and the effect of different parameters in bubble column experiments on the $k_L a$ values have been shown by several researchers. While column and sparger design (Shah et al. 1982), fluid properties (Alvarez et al. 2000), system pressure and temperature (Jin et al. 2014) all have an influence on the $k_L a$ value, several researchers and studies have agreed that $k_L a$ is primarily a function of superficial gas velocity alone and can be scaled up and correlated with velocity. The empirical correlation

developed based on superficial gas velocity alone was first presented by Deckwer et al. (1974) and shown in Equation 2.4:

$$k_L a = \alpha U_{SG}^{\beta} \quad [2.4]$$

In most literature studies, the relationship between $k_L a$ and U_G is less than linear resulting in a β between 0.70 and 0.92 while a few studies show that β varies in a narrow window between 0.80 – 1.15 making the relationship greater than linear (Besagni et al. 2018). The β exponent has been shown to be slightly influenced by the column size. For narrow columns ($D_c < 0.2$ m), which for most laboratory experimental studies including this study the column is considered narrow, $\beta < 1$. For industrial columns with larger column diameters ($D_c > 0.2$ m), there have been reported β values ranging from 1.00-1.15. Although there is a narrow window of exponent values, the slight variation in the exponent has shown to result in large variations in α (Deshpande et al. 2019). The study by Shah et al. (1982) reported two very different α values from 0.47 to 1.17 solely based on the change in sparger design. This result as well as the studied effect of sparger design, led to the development and use of coarse sparger types instead of fine sparger dispersers for this experimental study. Despite the small fluctuations in the two coefficients, α and β have been shown to be fairly scale insensitive.

The experimental results in this study show a significant influence of both superficial gas velocity and system pressure on the $k_L a$ values. Because of this and the research done by Lau et al. (2004) that showed the significant influence of pressure at higher superficial gas velocities, a $k_L a$ correlation will be developed in the form:

$$k_L a = A(U_G)^B \left(\frac{P}{P_{atm}} \right)^C \quad [2.5]$$

Through the experiment results, the coefficients A, B and C will be determined for the pressure ranges of 100-300 psig. The correlation, experimental conditions and results are presented in Table 8. Several previous literature experiments have neglected the influence of pressure and performed experiments at atmospheric conditions. For the application of this study, higher pressure conditions must be considered and the resulting correlation accounts for higher pressure ranges.

2.4. Previous Studies of Interfacial Area

For commonly used models with computation fluid dynamics (CFD), the prediction of interfacial area is one of the major weaknesses, emphasizing the importance of experimental determined values for specific interfacial area (Kiambi et al. 2001). Specific interfacial area has been the emphasis of several previous studies and has been experimentally determined using different physical and chemical methods. The most common physical methods that have been used are with optical probes, image analysis with video imaging and gas disengagement (Xue 2004). In all methods except for image analysis, the interfacial area is calculated as a function of gas holdup (ε_G) and Sauter mean diameter (d_s) of the bubbles by:

$$a = \frac{6\varepsilon_G}{d_s} \quad [2.6]$$

$$d_s = \frac{\sum_{i=1}^n n_i d_{b,i}^3}{\sum_{i=1}^n n_i d_{b,i}^2} \quad [2.7]$$

For the physical methods, excluding image analysis, the calculation of interfacial area in Equations 2.6-2.7 are based on the assumption that the bubbles in the multiphase system are spherical which is inaccurate. In this study, the use of image analysis was chosen to measure the interfacial area of bubbles as ellipsoid bubbles for improved accuracy. Considering all bubbles as

spherical is oversimplification and can only be used as a rough estimate, making the other physical methods of measuring interfacial area less accurate than the image analysis method. The chemical methods are based on kinetics of reactions and the absorption rate is a function of the interfacial area. This method has been used in several previous studies (Sada et al. 1987; Wilkinson et al. 1994); however, the chemical method is not an applicable method for studying interfacial area for methane in nonaqueous fluids. Table 2.4 shows several previous studies that investigated interfacial area using the various physical methods discussed. Because of the differences in operating conditions, methods and calculations, the experimental results of interfacial area differ significantly between studies and can be limited to a range of specific operating conditions.

Table 2.4. Previous literature studies using different techniques to calculate interfacial area

<i>Authors</i>	<i>Gas-Liquid</i>	<i>Pressure (psi)</i>	<i>U_{SG} (cm/s)</i>	<i>a (m^2/m^3) d_s (mm)</i>	<i>Technique</i>
<i>Bensler (1990)</i>	Air-Water	14.7	3.5-25.3	67.0-391.6 -	Photographic
<i>Hibiki et al. (2001)</i>	Air-Water	14.7	1.23-6.19	31.6-93.0 -	Photographic
<i>Akita and Yoshida (1974)</i>	Air-Water, Glycol Solutions	14.7	0.08-7.03	- 2.67-15.9	Photographic
<i>Hibiki et al. (1998)</i>	Air-Water	14.7	1.78-9.36	25.8-135 -	Probe
<i>Yun (1996)</i>	Steam-Water	14.7-100	0.29-13.8	11.6-161.0 -	Probe
<i>Hean et al. (1996)</i>	Air-Water	14.7	2.23-17.0	- 4.64-7.65	Dynamic Gas Disengagement
<i>Sada et al. (1987)</i>	O ₂ -Sodium Sulfite Solutions	14.7	1.6-20.5	- 5.1-8.2	Chemical
<i>Wilkinson et al. (1994)</i>	N ₂ , He, CO ₂ , SF ₄ – n- Heptane, mono- ethylene glycol	14.7	2.0-18.0	- 2.81-7.56	Chemical

Interfacial area is one of the main parameters that influence mass transfer in multiphase systems which makes it a crucial parameter to determine experimentally for future design and simulation work. Similarly, to the volumetric mass transfer coefficient, the interfacial area is affected by multiple parameters like column diameter, axial and radial direction, sparger design, gas velocity, flow regime and the gas and liquid properties. Previous studies have provided empirical correlations for the specific interfacial area, where Akita and Yoshida (1974) were one of the first using the photographic technique to develop a correlation:

$$a = \frac{1}{3D_H} \left(\frac{gD_H^2 \rho_L}{\sigma} \right)^{0.5} \left(\frac{gD^3}{v_L^2} \right)^{0.1} \varepsilon_G^{1.13} \quad [2.8]$$

The interfacial area correlation developed by Akita and Yoshida (1974) is a function of hydraulic equivalent diameter of the flow channel, viscosity and surface tension of the liquid and gas holdup. Most of the previous studies were conducted at atmospheric pressure as measurements of interfacial area are much more complicated at higher pressures (Xue 2004). As pressure is increased, there is bubble breakup and a decrease in bubble size that leads to an increase in overall interfacial area and gas holdup. Wilkinson, Spek and van Dierendonck (1992) experimentally developed a correlation to determine interfacial area at higher operating pressures based on gas holdup and density of gas at atmospheric and high-pressure conditions:

$$\frac{a \text{ (high pressure)}}{a \text{ (atmospheric)}} = \frac{\varepsilon_G \text{ (high pressure)}}{\varepsilon_G \text{ (atmospheric)}} \left(\frac{\rho_G \text{ (high pressure)}}{\rho_G \text{ (atmospheric)}} \right)^{0.11} \quad [2.9]$$

This correlation provides an estimate for the value of interfacial area at higher pressures if the known gas holdup and density values are known for the higher-pressure conditions. This developed relationship has been used as an estimate only and is not as accurate as using one of the physical methods to determine interfacial area experimentally. Due to the oversimplification of

estimating interfacial area with the assumption of spherical bubbles only, the preferred method for this experimental study is the photographic technique to accurately measure interfacial area. Once the values for interfacial area have been determined, the liquid-side mass transfer coefficient can also be investigated. Most previous studies have investigated volumetric mass transfer coefficient as one combined parameter but using the photographic technique the $k_L a$ values can be separated into interfacial area and k_L under different operating conditions.

Chapter 3. Experimental Development

In this chapter, the low and high pressure experimental mass transfer apparatuses, procedures, calculations and experimental designs will be discussed. Previous studies have not experimentally investigated the absorption mass transfer kinetics that could represent gas absorption scenarios in a riser or wellbore. The apparatuses were continuously upgraded throughout the experimental development as further parameters were investigated to better replicate the real downhole conditions of well control events.

3.1. Low Pressure Mass Transfer Apparatus

To measure the volumetric mass transfer coefficient at various experimental conditions, a bubble column ($H_c = 1.8$ meters) with 0.7112 meters of static liquid was used, as shown in Figure 3.1. For the absorption mass transfer coefficients to be comparable between experiments, the same temperature, liquid height, apparatus and procedures were used for consistency when determining the effect of multiple parameters on the $k_L a$ values. The initial experimental trials investigated the effect of superficial gas velocity, system pressure and fluid type. Two different pressures were used (100 and 200 psig), four different superficial gas velocities (0.45, 0.90, 1.68 and 2.51 cm/s) and two different fluid types (diesel and internal olefines). In later experiments, the ranges of the parameters were increased, and the investigation of further parameters were conducted.

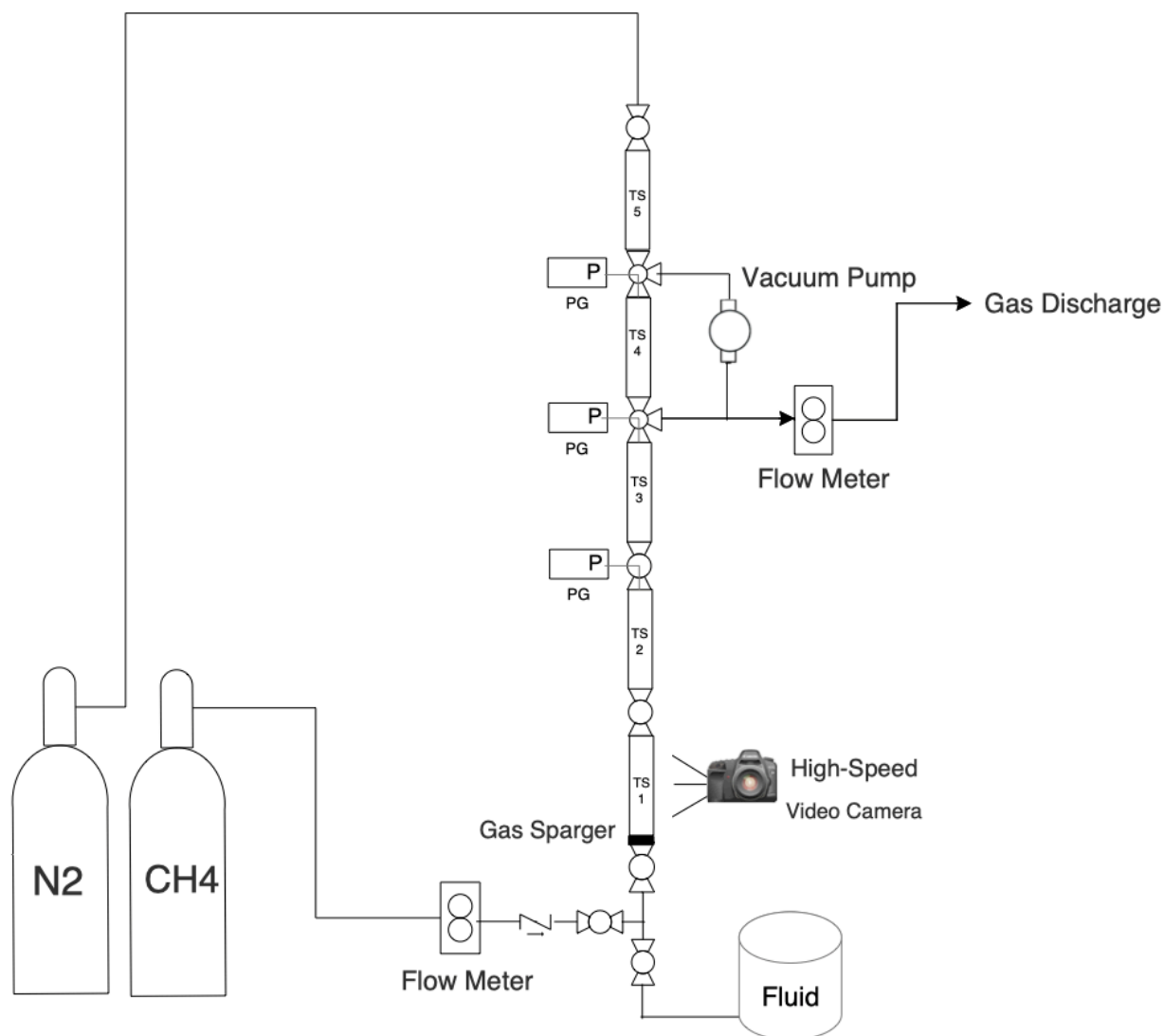


Figure 3.1. PFD of the low-pressure mass transfer experimental lab apparatus

Initially, the column in Figure 1 was empty and the vacuum pump was used to generate a vacuum within the experimental apparatus. Once a sufficient vacuum is generated, diesel or internal olefins were siphoned into TS1 and TS2 to fill both test sections completely. A nitrogen supply line connected at the top of the column was used to pressurize the column up to the desired experimental pressure (100-300 psi) before each test. Upon reaching the desired experimental pressure, the absorption experiment was ready to be conducted.

Using a regulator on the methane tank, the inlet at the bottom of TS1 was charged with methane to the same pressure as within the column before flowing methane through the fluid. The inlet and outlet valves were opened to allow the flow of methane through the diesel and absorption experiments are conducted for different durations of time from 30 seconds to 20 minutes. The inlet flow rate (1-25 l/min) can be controlled using the outlet valves on the column. The totalized volume of gas influx and the flow rate is recorded on the inlet flow meter.

The methane flows through the test section for the designated amount of time before the amount of gas absorbed into the diesel was recorded. After each time interval, TS1 and TS2 that contain the fluid was isolated stopping the flow of gas through the column. While TS1 and TS2 remain isolated, the vacuum pump was used on the column to remove any methane in the column to ensure the only measured methane flowing through the outlet flow meter is methane that was absorbed into the testing fluid. Once the column has a vacuum, the vacuum pump was used to pull the absorbed gas out of solution and through the outlet flow meter. The amount of gas that was absorbed in solution at each time interval is recorded until the maximum concentration for complete saturation of methane in the experimental fluid is reached. This procedure was repeated at each time step in the concentration vs time graph at each experimental pressure and superficial gas velocity of methane.

3.2. High Pressure Mass Transfer Apparatus

The high pressure experimental apparatus was designed to be able to perform the same experimental procedure in a very similar manner with much higher ranges of superficial gas velocity and pressure conditions. The new high pressure apparatus was built and delivered to the LSU Petroleum Engineering Research & Technology Transfer Laboratory in the Fall of 2019 and is shown in Figure 3.2. The apparatus is equipped with automated valves, a flow controller,

pressure regulators and liquid and gas pumps that allow for remote access control for safety and convenience reasons. The column diameter, $D_c = 2.625$, is larger than the low pressure apparatus allowing for the investigation of upscaling column diameter to see the influence on the mass transfer kinetics. The high pressure apparatus was built to allow pressure ranges up to 4500 psig, giving the ability to investigate a much larger range of experimental pressure conditions. The flow controller equipped on the inlet of the apparatus can accurately measure flow rates at standard conditions from 1-100 l/min compared to a maximum of 20 l/min on the low pressure apparatus. Following the investigation of mass transfer rates at low pressure and superficial gas velocity ranges, similar experiments were performed on the high pressure apparatus shown in Figures 3.2-3.3.



Figure 3.2. High-pressure apparatus currently installed at the LSU PERTT Laboratory

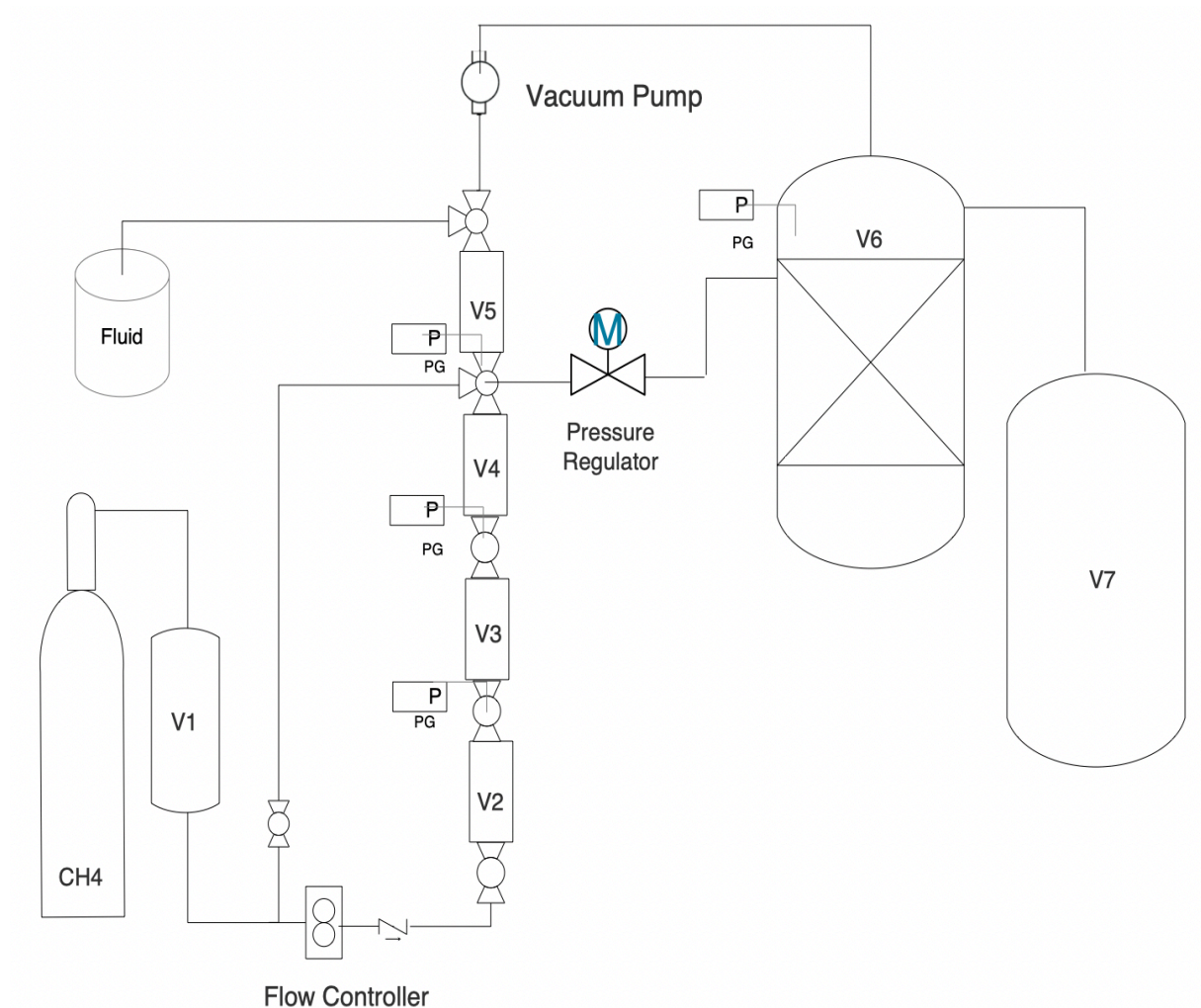


Figure 3.3. PFD of the high-pressure mass transfer experimental apparatus

Initially, the high pressure mass transfer apparatus was empty and the systems power was turned on allowing full remote access control of the apparatus from the testing center. Pump 2 was turned on to start the flow of testing fluid (water or internal olefins) into the test section filling up V2 and V3 with the necessary amount of liquid for absorption experiments. The system was isolation and the regulator on the gas cylinders (methane or CO₂) was set to the desired experimental pressure (200-1400 psi). Once V1 was brought to the desired testing pressure, FC1 was set to the desired experimental flow rate (later converted to superficial gas velocity). With the outlet closed to build pressure, the gas was injected through the flow controller at a constant flow

rate bringing the high pressure apparatus up to the desired pressure conditions.

Then the high pressure apparatus was at the desired testing conditions and the absorption experiments were ready to be conducted. On the outlet of the apparatus, there is a pressure regulator that acts as a choke to keep the apparatus at the operating pressure and flow rate as the gas is injected through the fluid and system. Once the pressure regulator is set, the outlet is opened allowing for a continuous controlled flow of gas through the liquid for absorption to take place. Several different experiments are conducted from 30 seconds to 20 minutes to generate a complete a curve of concentration of gas dissolved in the liquid until complete saturation is reached. After each time interval, V2 and V3 that contain the fluid was isolated stopping the flow of gas through the column. While V2 and V3 remain isolated, the vacuum pump was used on the column to remove any methane in the column to ensure the only measured methane flowing through the outlet flow meter is methane that was absorbed into the testing fluid. Once the column was drained except for the dissolved gas in solution, it was time to measure the amount of gas that was dissolved. The initial pressure of V6 was recorded and then the dissolved gas was removed from the liquid using a vacuum pump that empties the gas into V6. The amount of dissolved gas was measured by an initial and final pressure differential in V6. The amount of gas that was absorbed in solution at each time interval was recorded until the maximum concentration for complete saturation of gas in the experimental fluid was reached. This procedure was repeated at each time step in the concentration vs time graph at each experimental pressure and superficial gas velocity.

3.3. Materials and Fluid Characterization

The two nonaqueous-based fluids used in this study were No. 2 diesel fuel and a synthetic fluid provided by Halliburton which was comprised of a blend of internal olefins. The diesel used in this study was a common diesel blend used in drilling applications and automotive use. The

carbon compositions were found from a GC-MS analysis for both fluids and the results showed that diesel fluid ranged from C9-C23 in weight, while the carbon composition for the internal olefin blend was between C10-C19. Along with the fluids in this study, methane was used to determine the absorption mass transfer kinetics of methane into non-aqueous base fluids. The methane used in this study had a high purity of 99.95%. Pure nitrogen was also used as a blanket gas to bring the experimental apparatus up to the desired testing pressure. Table 3.1 shows the physical properties for each of the fluids used in this experimental study.

Table 3.1. Physical properties of diesel and internal olefin used in this study

Fluid	Density (kg/m ³)	Viscosity (40 °C, mm ² /s)	Aniline Point (°C)	Sulfur Content (ppm)	Color
Diesel	831.95	2.1	49	<500	Yellow
EDC 99-DW US Internal Olefin	815.90	2.4	79	<1	Clear

3.4. Volumetric Mass Transfer Coefficient Calculations

For each set of experimental tests to determine the absorption mass transfer coefficient at specific conditions, several sets of data were recorded and are shown in Appendix A in Table A.1. As methane flows through the testing fluid, diesel and internal olefin, the methane is absorbed into the fluid at various rates until complete saturation is reached. Figure 3.4 shows the total amount of methane (L) absorbed into the internal olefins at 100 psi and a range of superficial gas velocities. 1.6 liters of total gas was absorbed to reach complete saturation at 100 psi. Once the pressure was increased to 200 psi, the internal olefin fluid can hold approximately twice as much dissolved methane at 3.3 liters. The amount of gas absorbed into the experimental fluid was determined from the outlet flowmeter following the flow of gas through the fluid for different amounts of time.

Several tests ranging from 30 seconds to 20 minutes were conducted until complete saturation was reached at each gas velocity.

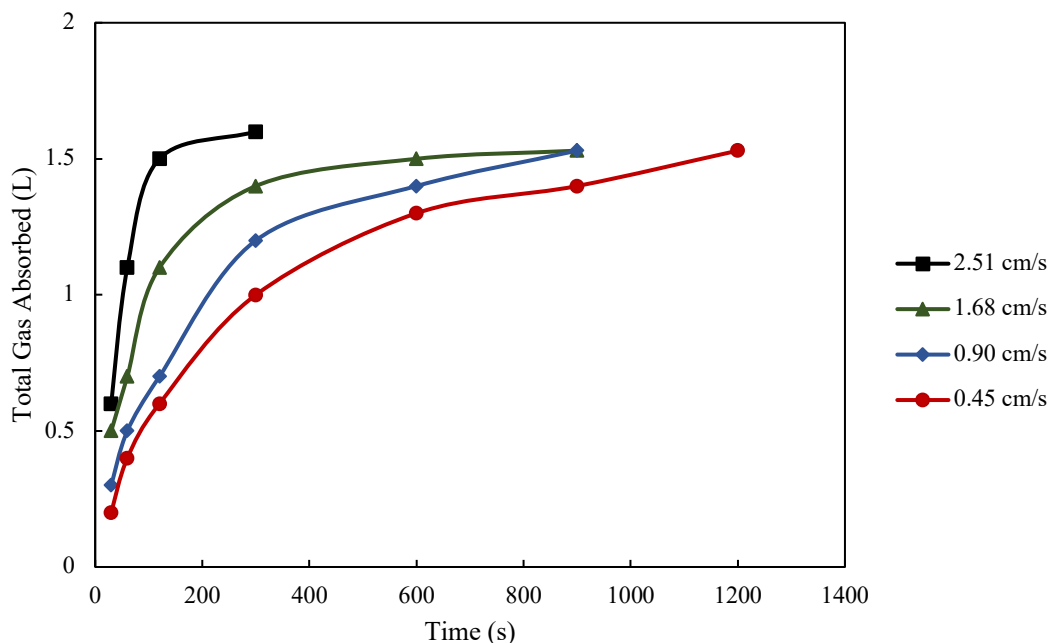


Figure 3.4. Total gas absorbed (L) of methane in internal olefin fluid at 100 psi and superficial gas velocities ranging from 0.45 to 2.51 cm/s

After the total amount of absorbed gas (L) is determined in Figure 3.4, the concentration of methane dissolved into 0.65 liters of internal olefins was calculated. Figure 3.5 shows that as the gas begins to flow through the pure fluid, the concentration of gas dissolved into liquid increases rapidly within the first 2 minutes at each gas velocity. At high gas velocities, complete saturation is reached within 3 minutes, while at low gas velocities it takes several minutes before saturation is reached. The difference between the maximum concentration and the concentration of gas in liquid at a specific time becomes less as complete saturation is approached. As the saturation limit is approached, the rate of absorption slows as less gas can be dissolved into the liquid at that point.

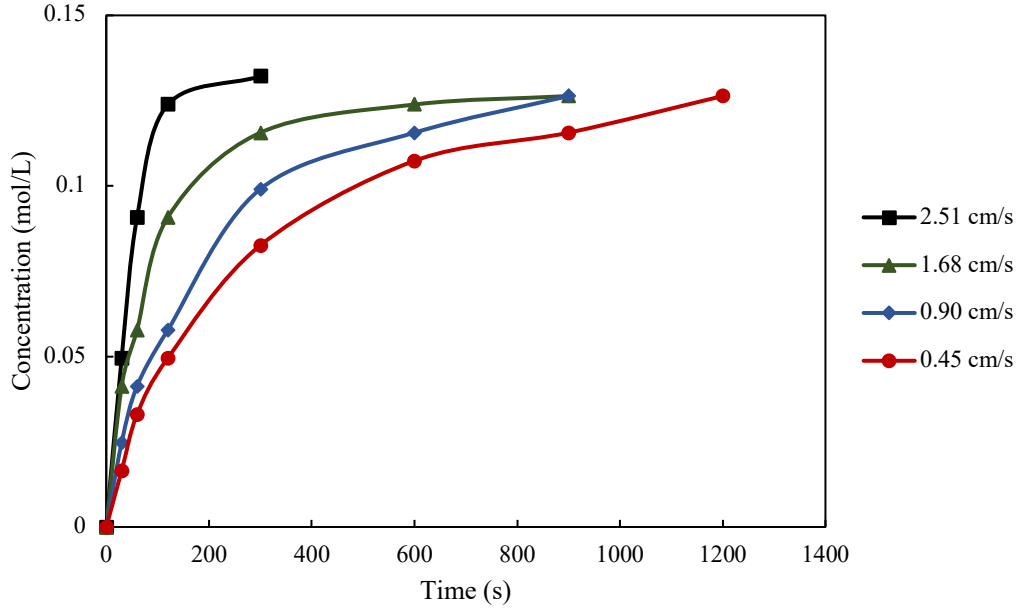


Figure 3.5. Concentration of methane (mol/L) dissolved into internal olefin fluid over time at 100 psi and superficial gas velocities ranging from 0.45 to 2.51 cm/s

As previously discussed, following Equations 1.1-1.3 allows for the calculation of time dependent $k_L a$ values as a function of concentration of gas, maximum saturation concentration and time. In the experimental data, the value of $\ln\left(\frac{C^*}{C^* - C_L}\right)$ at each time interval from 0.5-20 minutes for each superficial gas velocity is calculated. The concentration (C_L) at each time interval is recorded until the maximum concentration (C^*) or complete saturation is reached. In Figure 3.6, the absorption mass transfer coefficient can be obtained from the linear slope on the graph of $\ln\left(\frac{C^*}{C^* - C_L}\right)$ vs time. At higher superficial gas velocities, the slope of the graph of $\ln\left(\frac{C^*}{C^* - C_L}\right)$ vs time increases because complete saturation is reached in a short amount of time. As a result, $k_L a$ increases with an increase in superficial gas velocities at constant pressure conditions.

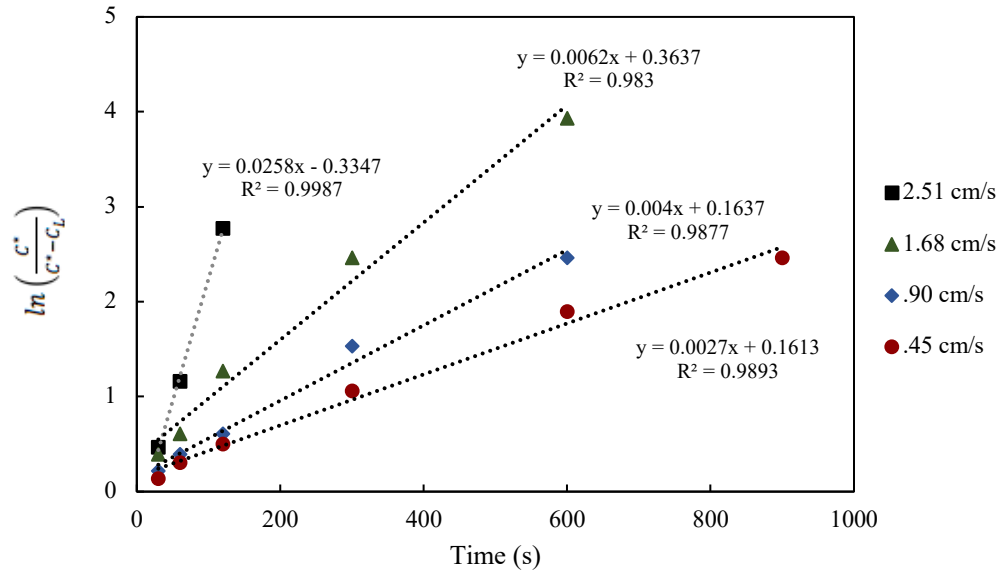


Figure 3.6. Graph of $\ln\left(\frac{c^*}{c^*-c_L}\right)$ vs time (s) for the calculation of $k_L a$ for methane in internal olefin fluid at 100 psi and superficial gas velocities ranging from 0.45 to 2.51 cm/s

3.5. Image Analysis Calculations

In this study, the calculation of the $k_L a$ values for different superficial gas velocities and system pressures will lead to the calculation of the liquid-side mass transfer coefficient and interfacial area. In previous studies, it has been difficult to separate the $k_L a$ values and accurately predict the liquid-side mass transfer coefficient and interfacial area. The photographic method has recently been used by Ahmed et al. (2015) and Feng et al. (2019) to calculate gas holdup and interfacial area in gas-liquid systems and the same method was used in this study to separate the volumetric mass transfer coefficient.

During the experimental process, a high-speed video camera was used and image analysis was performed at each superficial gas velocity and system pressure to determine the volumetric mass transfer coefficient, liquid-side mass transfer coefficient and the gas-liquid interfacial area. A Sony DSC-RX10M2 camera and ImageJ image processing software were used to capture and

analyze the slow-motion videos taken. To analyze the images taken during the experiments, they are first uploaded to the ImageJ processing software where the images can be enhanced for improved calculations. The 148–486-pixel images were first set to scale using the column diameter of 0.0254 meters, resulting in a scale of 5236 pixels/meter. The images shown in Figure 3.7 were enhanced in gray scale where the brightness and contrast were adjusted to improve the quality of the outlines of the bubbles within the column. Once the photographs were enhanced, calculations to determine the liquid-gas interfacial area were performed.

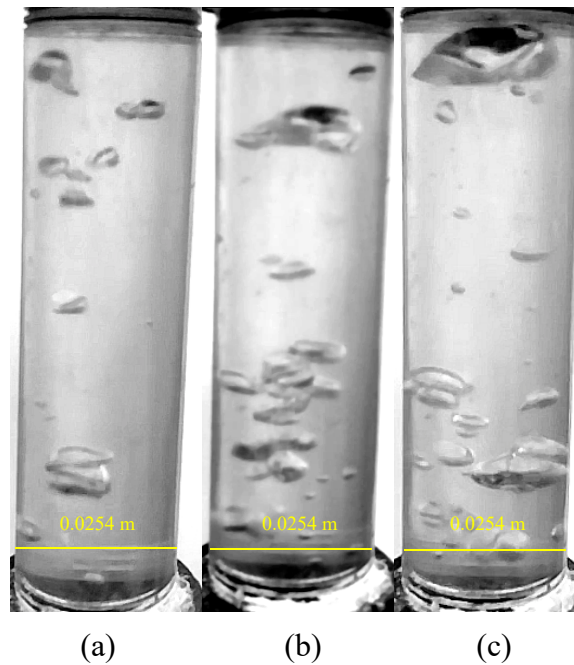


Figure 3.7. Processed experimental images with increased superficial gas velocity. (a): Image of bubble size distribution at $U_{SG} = 0.0045$ m/s. (b): Image of bubble size distribution at $U_{SG} = 0.0168$ m/s. (c): Image of bubble size distribution at $U_{SG} = 0.0491$ m/s.

For multiphase flow in bubble columns there are two flow common flow regimes encountered, bubble flow and churn-turbulent flow. Figure 3.7, shows the flow regime as bubble flow at low superficial gas velocities, but churn-turbulent flow becomes common when there is an increase in superficial gas velocity. At low superficial gas velocities, the bubble size distribution is more uniform and spherical bubbles exist. As shown in Figure 3.7, with a higher superficial gas

velocity, both bubble coalescence and breakup become evident and spherical bubbles start to become ellipsoidal and then spherical cap shaped as superficial gas velocity increases even further (Xue 2004). Each individual bubble in the column was initially treated as a two-dimensional object and the software was able to calculate a maximum and minimum axis diameter for each bubble. The bubbles were considered as ellipsoid when calculating surface area and volume of the bubbles. Figure 3.8 shows the justification of considering the bubbles as ellipsoids and the side view of the column justifies the use of the maximum axis diameter in a two-dimensional image as the third diameter.

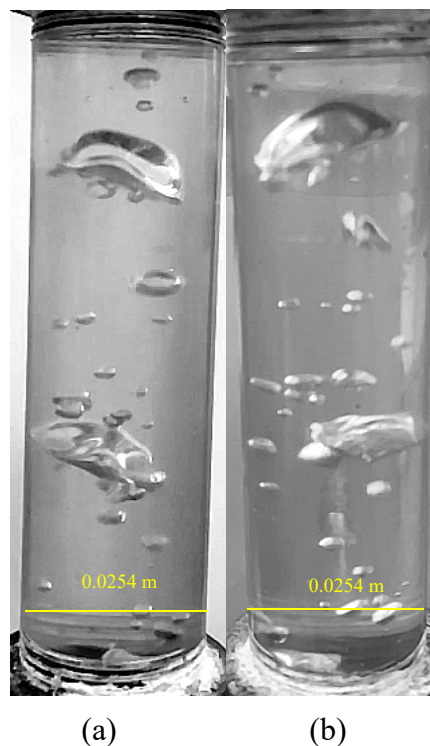


Figure 3.8. Experimental images for ellipsoidal bubble calculation assumption. (a): Front view of the experimental apparatus. (b): Side view of the experimental apparatus.

Once the minimum (a) and maximum (b and c) axis diameters for each bubble within the column were determined, the surface area and volume of the ellipsoid bubbles were calculated:

$$S = 4\pi \left(\frac{(ab)^{1.6} + (ac)^{1.6} + (bc)^{1.6}}{3} \right)^{1/1.6} \quad [3.4]$$

$$V_B = \frac{4}{3} \pi abc \quad [3.5]$$

The sum of the surface area and sum of the volume of ellipsoid bubbles allows for the calculation of gas holdup and interfacial area (a). Gas holdup in a bubble column is known as the summation of the total volume of the gas phase in the total volume of the liquid and interfacial area is calculated using the using the surface area of the bubbles per total liquid volume:

$$\varepsilon_G = \frac{\sum V_B}{V_c} \quad [3.6]$$

$$a = \frac{\sum S}{V_c} \quad [3.7]$$

Once the volumetric mass transfer coefficient is determined for each experiment and the analyzed images give the resulting interfacial area, the liquid-side mass transfer coefficient (k_L) can be calculated:

$$k_L = \frac{k_L a}{a} \quad [3.8]$$

The calculations from the image analysis method and image processing software were necessary to allow for accurate determination of both k_L and a , where several previous studies have only investigated $k_L a$ as one single parameter or measured interfacial area using other physical methods.

3.6. Validation of Image Analysis Measurements

Using the photographic method and calculations previously discussed, the interfacial area for experimental condition was determined. With the absorption experiments taking place over a given length of time, the consistency and accuracy of interfacial area calculations over the duration of

the experiments needed to be verified. Figure 3.9 shows the determined interfacial area from image analysis over 180 seconds of recorded data for an experiment at 100 psi and a superficial gas velocity of 0.0090 m/s. The average interfacial area was 31.77 m^{-1} with a percent error of $\pm 14\%$ from the average. The calculations using the ellipsoid bubble equations results in a consistent and accurate measurement of interfacial area throughout the length of each experimental test. The average interfacial area was calculated for each experimental testing conditions to ensure that an accurate value was determined in the results section. Figure 3.10 shows the photographs taken with the high-speed video camera at each time interval during the duration of the experimental test which corresponds with the first 120 seconds of data points in Figure 3.9.

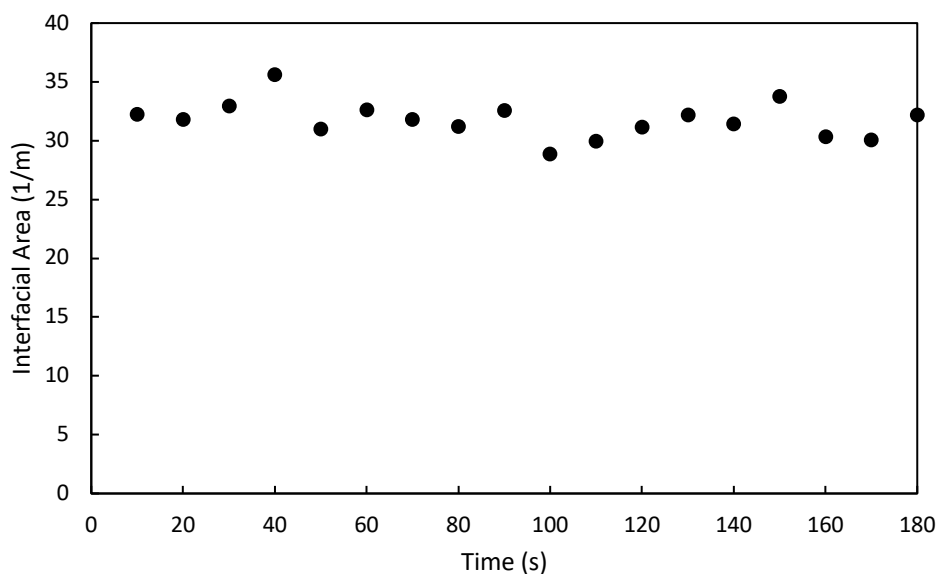


Figure 3.9. Interfacial area in 10 second time intervals during the experimental test at 100 psi and 0.0090 m/s

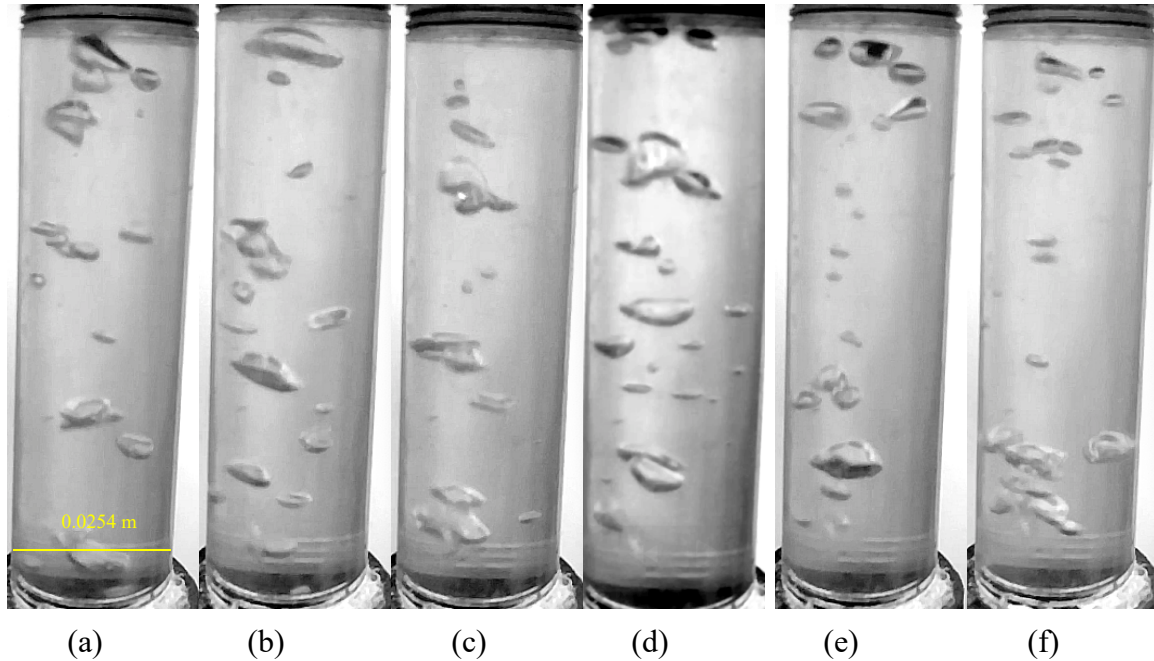


Figure 3.10. Images for interfacial area in 20 second time intervals at 100 psi and 0.0090 m/s. (a): 20 seconds. (b): 40 seconds. (c): 60 seconds. (d): 80 seconds. (e): 100 seconds. (f): 120 seconds.

Figure 3.9 shows the calculated values for interfacial area using the spherical and ellipsoidal bubble equations previously discussed. Equations 2.6-2.7 are under the assumption that the bubbles in the bubble column are spherical which is not true for most multiphase systems (Xau 2004). As superficial gas velocity increases, the bubbles transition from bubbly flow with spherical bubble size to churn-turbulent flow with ellipsoidal bubbles. Calculating interfacial area as a function of gas holdup and Sauter bubble diameter is an oversimplification when assuming constant spherical bubbles. With the increase in superficial gas velocity, the calculations using spherical bubble equations leads to an over estimation of interfacial area as shown in Figure 3.11. For an accurate measurement of interfacial area under all operating conditions, Equations 3.4-3.7 are used assuming ellipsoidal bubbles.

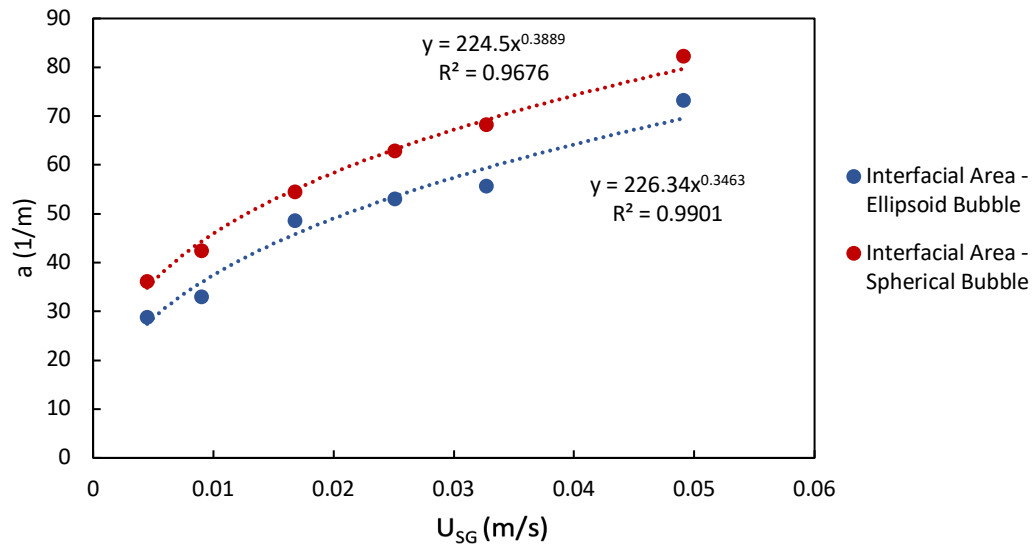


Figure 3.11. Interfacial area values for assumption of spherical and ellipsoid bubbles

3.7. Experimental Design for Investigation of Parameters

3.7.1. The Effect of Pressure, Superficial Gas Velocity and Fluid Type

With the current experimental mass transfer apparatus, Table 3.2 shows the initial experimental test matrix used to investigate the effects of system pressure, superficial gas velocity and fluid type on the $k_L a$ values:

Table 3.2. Experimental test matrix for the investigation of pressure, superficial gas velocity and fluid type

Test	Base Fluid	Pressure, MPa (psig)	U_{SG} (cm/s)
1	Diesel	0.69 (100)	0.45
2			0.90
3			1.68
4			2.51
5		1.38 (200)	0.45
6			0.90
7			1.68
8			2.51

(table cont'd.)

<i>Test</i>	<i>Base Fluid</i>	<i>Pressure, MPa (psig)</i>	<i>U_{SG} (cm/s)</i>
9	IO	0.69 (100)	0.45
10			0.90
11			1.68
12			2.51
13		1.38 (200)	0.45
14			0.90
15			1.68
16			2.51

The effects that pressure, superficial gas velocity of methane, and the type of base fluid have on the absorption mass transfer coefficient are determined within the experimental scope of work of this paper. The 16 experimental tests were conducted to calculate the mass transfer coefficient at pressures of 100 and 200 psig, superficial gas velocities of 0.45, 0.90, 1.68 and 2.51 cm/s and base fluid of diesel and internal olefins. Once the mass transfer coefficient was calculated for these 16 experiments, the effects of increasing the experimental pressure, gas velocity or changing base fluid type on the $k_L a$ value while holding the other factors constant could be determined.

3.7.2. The Effect of Sparger Design

Once the effects of pressure, superficial gas velocity and fluid type were investigated, the influence of other parameters could be investigated. Table 3.3 shows the test matrix for the investigation of sparger design on the $k_L a$ values. Three different sparger types were used in the test matrix: a single hole orifice ($D_o = 8.89$), a coarse sparger distributor ($D_o > 2.0$ mm) and a fine sparger distributor ($D_o < 2.0$ mm). The effect of sparger type with increased superficial gas velocity under similar experimental testing conditions were tested in Table 3.3 and the results discussed further.

Table 3.3. Experimental test matrix for the investigation of sparger design

<i>Test</i>	<i>No. of Holes</i>	<i>Sparger Diameter (mm)</i>	<i>U_{SG} (cm/s)</i>
1	1	8.89	0.9
2	5	3.56	0.9
3	5	3.56	1.68
4	5	1.8	0.9
5	10	1.8	0.9
6	10	1.8	1.68

Figure 3.12 shows the designed perforated plates that were used in this experimental investigation and inserted at the bottom of the apparatus. Bubble size was varied using 4 different sparger plates ranging from 1 single hole to a perforated 10-hole sparger. The sparger hole diameters ranged from $D_o = 8.89$ mm (single tube sparger), $D_o = 3.56$ mm (coarse sparger) to $D_o = 1.80$ mm (fine bubble sparger). Having one sparger with 5 holes and another with 10 holes at the same sparger diameter ($D_o = 1.80$) also allowed for the investigation of rise velocity under the same superficial gas velocity conditions.

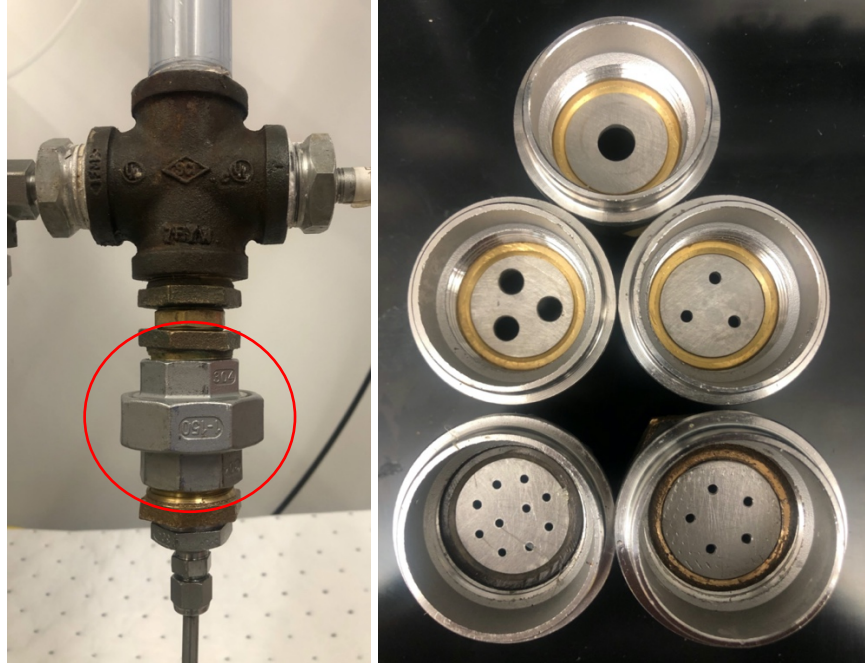


Figure 3.12. Images of the sparger designs on the experimental apparatus

3.7.3. The Effect of Column Diameter

The effect of column diameter was experimental investigated using both the low pressure and high pressure mass transfer apparatus. The column diameters for the low and high pressure apparatus are 1.0 in. and 2.625 in. respectively. Table 3.4 shows the 4 tests performed on each apparatus, with all 8 of the tests performed with the same operating pressure and superficial gas velocity to determine the effect of column diameter alone.

Table 3.4. Experimental test matrix for the investigation of column diameter

<i>Test</i>	<i>Pressure, MPa (psig)</i>	<i>Column Diameter (in)</i>	<i>Flow Rate (ln/min)</i>	<i>U_{SG} (m/s)</i>
1	1.38 (200)	1.0	2.00	0.0045
2			4.00	0.0090
3			7.48	0.0168
4			11.23	0.0251

(table cont'd.)

<i>Test</i>	<i>Pressure, MPa (psig)</i>	<i>Column Diameter (in)</i>	<i>Flow Rate (ln/min)</i>	<i>U_{SG} (m/s)</i>
5	1.38 (200)	2.625	8.03	0.0045
6			15.92	0.0090
7			29.80	0.0168
8			44.55	0.0251

The experimental tests were conducted with an operating pressure of 200 psi and superficial gas velocity ranging from 0.0045-0.0251 m/s. The flow rates are shown on the flow meters for each apparatus in units of normal liters (ln) per minute which is the flow rate at standard pressure and temperature conditions. The standard flow rate is then used to convert to the same superficial gas velocity between the 2 testing columns despite the difference in column diameter. The normal liters per minute is converted to liters per minute by using the Boyle's Law and the calculating the volume of gas under the elevated pressure condition. From the volumetric flow rate, the superficial gas velocity can be calculated from the area of the apparatus. The results of this experiment will lead to the understanding of the influence of column diameter on mass transfer kinetics and the ability to scale up the results to larger diameters for industry applications and simulations of well control events.

3.7.4. The Effect of Elevated Pressure

With the development of the high pressure apparatus, the effect of elevated operating pressure higher than 300 psig could be investigated. For well control events and riser gas migration scenarios, the operating conditions will be at elevated pressure conditions. Table 3.5 shows the test matrix to determine the effect of elevated pressure comparing the volumetric mass transfer coefficients between 200 and 800 psi and equivalent superficial gas velocities. Due to limitations of methane supplies, 800 psi was the highest experimental pressure used despite the high pressure

apparatus being rated for much higher pressures. Further tests at pressures above 800 psi could be conducted in the future with a sufficient gas supply.

Table 3.5. Experimental test matrix for the investigation of elevated pressure

<i>Test</i>	<i>Pressure, MPa (psig)</i>	<i>Flow Rate (ln/min)</i>	<i>U_{SG} (m/s)</i>
1	1.38 (200)	2.00	0.0013
2		4.00	0.0026
3		7.48	0.0045
4		11.23	0.0090
5	5.52 (800)	8.03	0.0013
6		15.92	0.0026
7		29.80	0.0045
8		44.55	0.0090

Chapter 4. EXPERIMENTAL RESULTS

In Chapter 4, the experimental results from the test matrixes in the previous chapter are presented. The measurement of solubility of methane in base fluids was the first experimental test conducted as the concentration values were used in the calculation of $k_L a$ values for the remaining experiments. The results for the influence of operating pressure, superficial gas velocity, fluid type, column diameter and sparger design are shown.

4.1. Solubility of Methane in Base Fluids

It was important to begin the experimental study by measuring the solubility of methane in diesel and internal olefins to accurately determine the maximum concentration of gas in solution at the various operating pressures. This concentration is important because it is used in the model presented in Equations 1.1-1.3 to calculate the volumetric mass transfer coefficient. Figure 4.1 shows the solubility experimental determined for the concentration of methane in solution at pressures ranging from 50 to 300 psi. The results of the series of saturation experiments shows that the solubility of methane in diesel is higher than the solubility in internal olefins. This is an important conclusion for further understanding of the interaction of methane and non-aqueous base fluids. Once the solubility is determined under different conditions, the influence of various parameters on the mass transfer coefficient can be investigated.

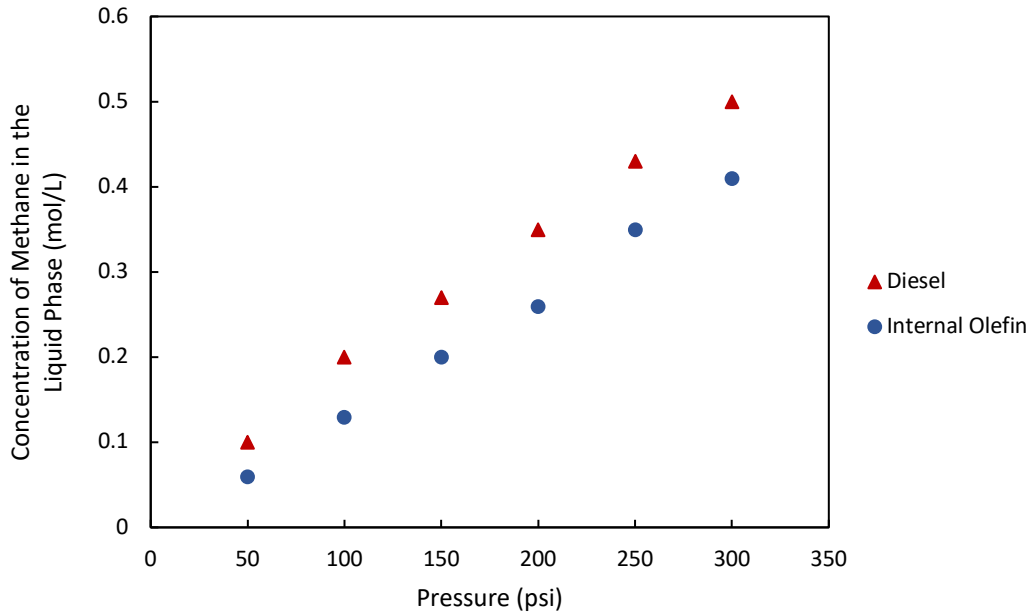


Figure 4.1. The concentration of methane in diesel and internal olefins at complete saturation at a temperature of 295 K and various pressures ranging from 50 to 300 psi.

4.2. The Effect of Pressure, Superficial Gas Velocity and Fluid Type

The effects of superficial gas velocity, system pressure and base fluid type on the $k_L a$ value were determined from the experimental test matrix. An initial design of 16 experimental tests were conducted as a proof of concept to investigate parameters with the mass transfer apparatus. The resulting $k_L a$ values from the experimental test matrix are shown in Figure 4.2. At constant pressures of 100 and 200 psig, the $k_L a$ value increases as the superficial gas velocity increases from 0.45 to 0.9 cm/s. The increase in superficial gas velocity under constant pressure conditions leads to a significant increase in interfacial area due to bubble breakup. Like with increasing gas velocity, the $k_L a$ value also increases with increasing system pressure as the superficial gas velocity is held constant. With an increase in superficial gas velocity, the increase in pressure leads

to bubble breakup and a reduction in bubble size with increased number of bubbles leading to a larger interfacial area and $k_L a$ values. There are many effects that may play a role in the increase in $k_L a$ with increasing pressure including compressibility, interfacial tension and density. Further studies should be done to identify the key parameters causing bubble breakup with higher operating pressure. The effects of these 2 parameters on the absorption coefficient is the same for methane in both diesel and internal olefin fluids. For all experimental conditions, the $k_L a$ value is larger for methane in diesel than the $k_L a$ value for methane in internal olefins. Along with methane and diesel having larger mass transfer rates, methane in diesel had a significantly higher solubility and about twice as much methane was dissolved in diesel than internal olefins at similar pressure conditions.

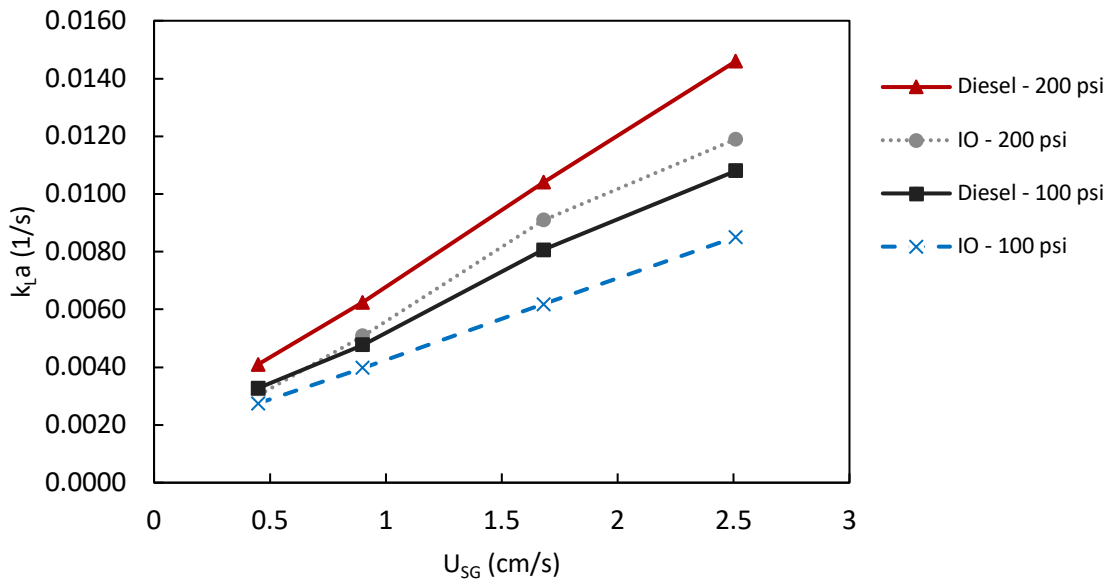


Figure 4.2. Experimental results for the effects of superficial gas velocity, system pressure and fluid type on $k_L a$ for methane absorption in non-aqueous fluids

Because of the results from the literature study of Lau et al. (2004) indicating that pressure had a more significant effect at higher superficial gas velocities, additional experiments were

performed with a larger range of superficial gas velocities and pressures using methane and internal olefins. The experimental results at higher pressure and superficial gas velocities ranges are shown in Figure 4.3.

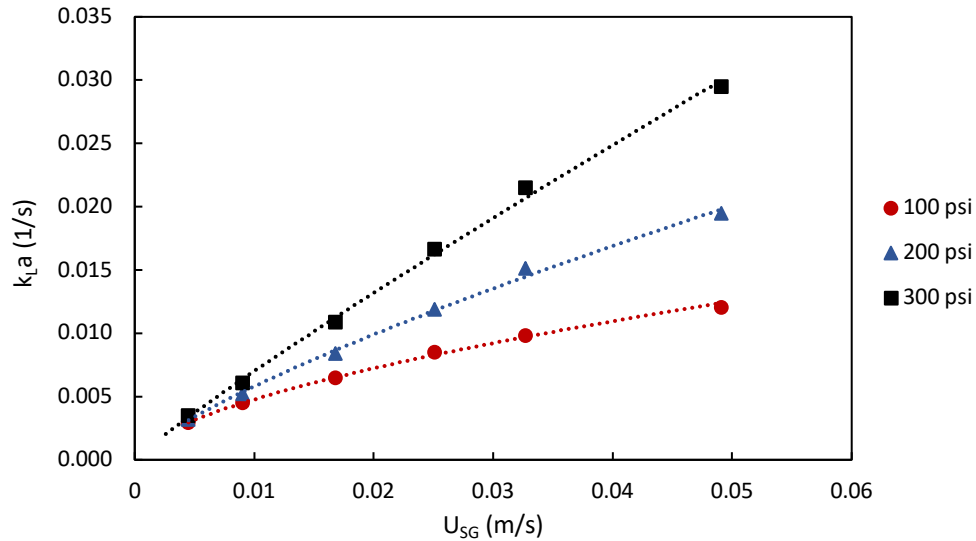


Figure 4.3. Experimental results for the effects of an increased range of superficial gas velocity (0.0045-0.049 m/s) and system pressure (100-300 psi) on k_La for methane absorption in nonaqueous fluids

4.3. The Effect of Sparger Design

Table 4.1. Experimental results for the effect of sparger design on k_La values

<i>Test</i>	<i>No. of Holes</i>	<i>Sparger Diameter (mm)</i>	<i>Total (mm)</i>	<i>U_{SG} (m/s)</i>	<i>Sparger k_La</i>	<i>No Sparger k_La</i>	<i>% Difference</i>
1	1	8.89	8.89	0.9	0.0032	0.00303	5.61%
2	5	3.56	17.78	0.9	0.00522	0.00508	2.76%
3	5	3.56	17.78	1.68	0.00838	0.0091	7.91%
4	5	1.8	8.89	0.9	0.007	0.00508	37.80%
5	10	1.8	17.78	0.9	0.0078	0.00508	53.54%
6	10	1.8	17.78	1.68	0.0168	0.0091	84.62%

Table 4.1 shows the experimental results from the investigation of the influence of sparger design on the absorption mass transfer coefficient. 6 experimental tests were conducted with 4

different sparger types and those results were compared to similar testing conditions without a sparger attached to the apparatus (No Sparger $k_L a$). For the applicability of scaling up $k_L a$ values and ensuring there is no significant influence of sparger design on the mass transfer coefficient, a coarse sparger design is needed ($D_o > 2.0$ mm). The first 3 experimental tests were conducted using this coarse sparger design, both with a multi-hole sparger and a single hole sparger. The results from those experiments, even after increasing the superficial gas velocity, were within $\pm 8.00\%$ of the $k_L a$ values from the experiments conducted without a sparger. However, experimental test 4-6 used a fine bubble sparger ($D_o < 2.0$ mm), which from literature is known to cause a significant effect on the mass transfer coefficient. With a fine bubble sparger, the sparger design has a smaller effect at low superficial gas velocities, but as the superficial gas velocity is increased it has a more significant effect (Test 6). Test 5, with a fine bubble sparger at a low superficial gas velocity had a $k_L a$ value that was 53.54% higher than the $k_L a$ value with no sparger on the apparatus. Once the superficial gas velocity was increased (Test 6), the $k_L a$ value was 84.62% higher than the value from the experiment with no sparger. This validates the use of the coarse bubble sparger for future experimental work and shows that using a fine bubble sparger will significantly influence the mass transfer coefficient. The use of a coarse bubble sparger will help improve consistency of bubble size distribution for each experiment and allow for easier calculation of interfacial area in future experimental studies.

4.4. The Effect of Column Diameter

According to Akita and Yoshida (1973) the $k_L a$ values can be related to column diameter up to a diameter of 0.15 meters. Wilkinson et al. (1992) stated 3 key criteria for scaling up mass transfer coefficient results and to remove the influence of bubble column dimensions when scaling up from a laboratory scale. As it has been noted in previous literature studies (Deshpande et al.

2019) that a large diameter column might not be practical in a laboratory setup, experiments and the mass transfer coefficient results can be scaled up using a $D_c < 0.15$ m if the flow regime is kept consistent and not in the slug flow regime. The 8 experimental tests were conducted using the low and high pressure apparatus with column diameters of 1.0 inch and 2.625 inches respectively. According to the results shown in Figure 4.4, there is only a minimal effect of column diameter on the resulting $k_L a$ values. Under the same experimental operating conditions, the $k_L a$ values for both column diameters are nearly equivalent. These experimental results are critical in the future work of scaling up mass transfer coefficient values to larger diameter systems for simulating gas influx management in wellbore and risers.

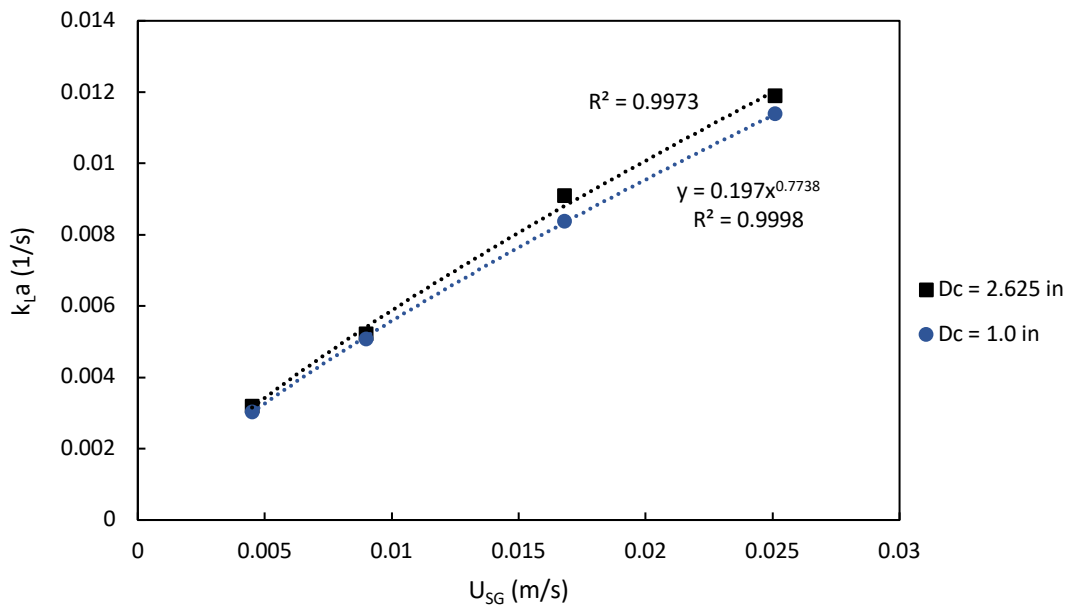


Figure 4.4. Experimental results for the effect of column diameter on $k_L a$ for methane absorption in non-aqueous fluids

4.5. The Effect of Elevated Pressure

Only a few previous literature studies have investigated the effect of elevated pressure conditions on the volumetric mass transfer coefficient (Lau et al. 2004; Jin et al. 2014) and most

developed correlations do not consider the effect of pressure. However, for the applications of this study, elevated pressure conditions must be investigated for gas influx management scenarios that have high operating pressure in the wellbore and riser. On the high pressure experimental apparatus, tests were performed at 200 and 800 psi with an increase in superficial gas velocity and the results from the 8 experimental tests are shown in Figure 4.5. The 200 psi tests were performed again on this apparatus for the comparison of column diameter, ability to scale up, and as a baseline of test repeatability between various columns. The results compared to the tests at the same operating conditions on the low pressure apparatus were previously shown. For the increase of pressure from 200 to 800 psi there is a significant increase in $k_L a$ values and it follows the same trend as the lower pressures. With a low superficial gas velocity, pressure does not influence the $k_L a$ values, but as superficial gas velocity increases the pressure has a very significant influence on $k_L a$.

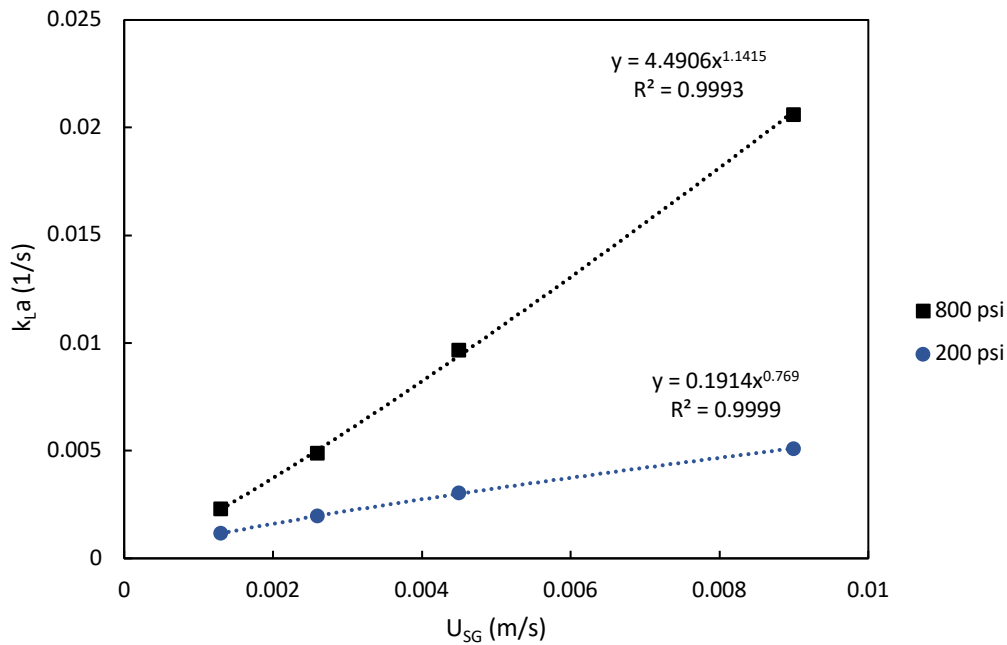


Figure 4.5. Experimental Results for the effect of elevated pressure on $k_L a$ for methane absorption in non-aqueous fluids

Chapter 5. DATA ANALYSIS

Following the parametric study and presentation of experimental results, the data was further analyzed in Chapter 5. The data analysis led to the development of a correlation for $k_L a$ based on the outcome of the experimental results. Further image analysis discussed in this section also led to the separation of the $k_L a$ values into the liquid-side mass transfer coefficient and interfacial area.

5.1. Development of $k_L a$ Correlation

Following the completion of the investigation of the influence of several different parameters on the volumetric mass transfer coefficient, Table 5.1 was conducted to develop a correlation for $k_L a$.

Table 5.1. Experimental test matrix for $k_L a$ correlation

<i>Test</i>	<i>Pressure, MPa (psig)</i>	<i>U_{SG} (m/s)</i>	<i>Flow Rate (ln/min)</i>
1	0.69 (100)	0.0045	1.07
2		0.0090	2.14
3		0.0168	4.00
4		0.0251	6.00
5		0.0327	7.80
6		0.0491	11.70
7	1.38 (200)	0.0045	2.00
8		0.0090	4.00
9		0.0168	7.48
10		0.0251	11.23
11		0.0327	14.61
12		0.0491	21.91
13	2.07 (300)	0.0045	2.93
14		0.0090	5.86
15		0.0168	10.97
16		0.0251	16.46
17		0.0327	21.41
18		0.0491	32.11

While column and sparger design (Shah et al. 1982), fluid properties (Alvarez et al. 2000), system pressure and temperature (Jin et al. 2014) all have an influence on the $k_L a$ value, several researchers and studies have agreed that $k_L a$ is primarily a function of superficial gas velocity alone. Additional experiments were conducted at a larger range of superficial gas velocities to increase the accuracy of developed correlations. Because pressure had a noticeable influence on $k_L a$ at higher superficial gas velocities, the correlations was modified from previous literature studies to include the effect of pressure on the volumetric mass transfer coefficient. This understanding is backed by previous research of Lau et al. (2004) who showed at low superficial gas velocities pressure does not have an influence on $k_L a$, but at higher superficial gas velocities the influence of pressure is very noticeable. The developed correlation to describe the volumetric mass transfer coefficient is in the form shown in Equation 2.5. Figure 5.1 and Table 5.2 shows the developed correlation based on the experimental results and the very specific experimental pressure and superficial gas velocity conditions used to determine the correlation.

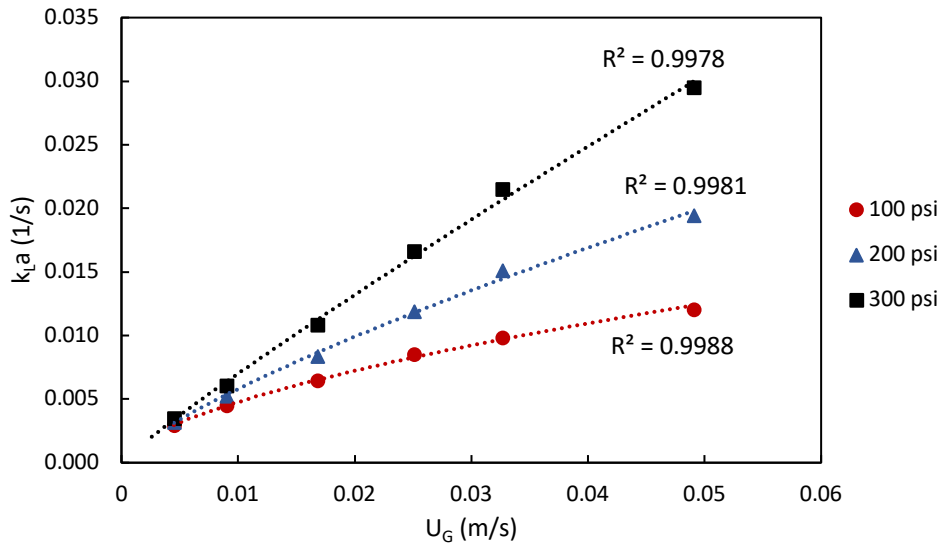


Figure 5.1. Experimental results for development of $k_L a$ correlation

Table 5.2. Range of experimental conditions for developed $k_L a$ correlation

<i>Conditions</i>	<i>Pressure (psig)</i>	<i>$k_L a$ Correlation</i>
<i>Methane-Internal Olefin; $D_c = 0.0254$ m; $H_c = 0.7112$ m; $U_{SG} = 0.0045$-0.0491 m/s; Coarse Bubble Sparger $D_o = 3.56$ mm</i>	100-300	$k_L a = A(U_{SG})^B \left(\frac{P}{P_{atm}} \right)^C$ A=0.0372 B=0.8199 C=0.7315

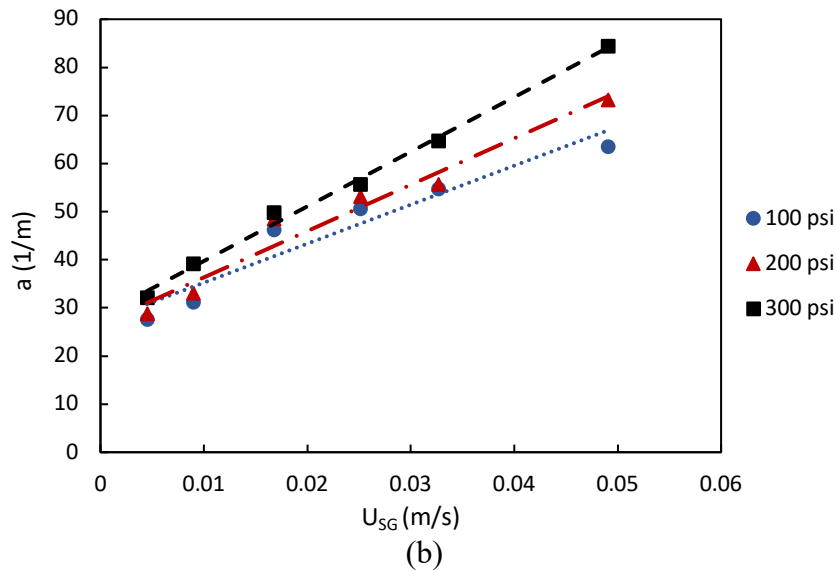
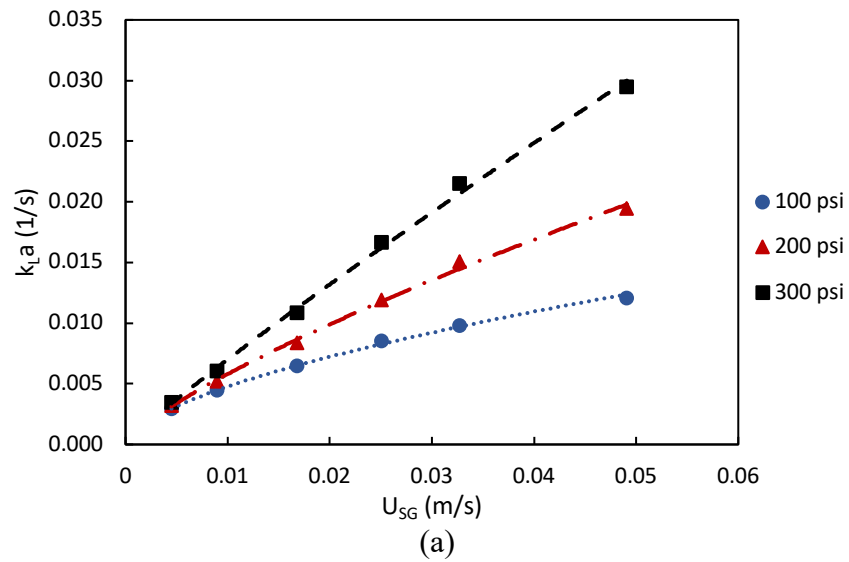
The ranges of the coefficients A, B and C are similar to previous studies and it is shown that a slight deviation in B can have a significant impact on the variation of A when a small range of superficial gas velocity is used in experimental development. For a temperature of 295 K and pressures ranging from 100-300 psig, A=0.0372, B=0.8199 and C=0.7315. The outcome of the developed correlation agrees with previous research studies and show that superficial gas velocity and system pressure have a significant influence on the volumetric mass transfer coefficient.

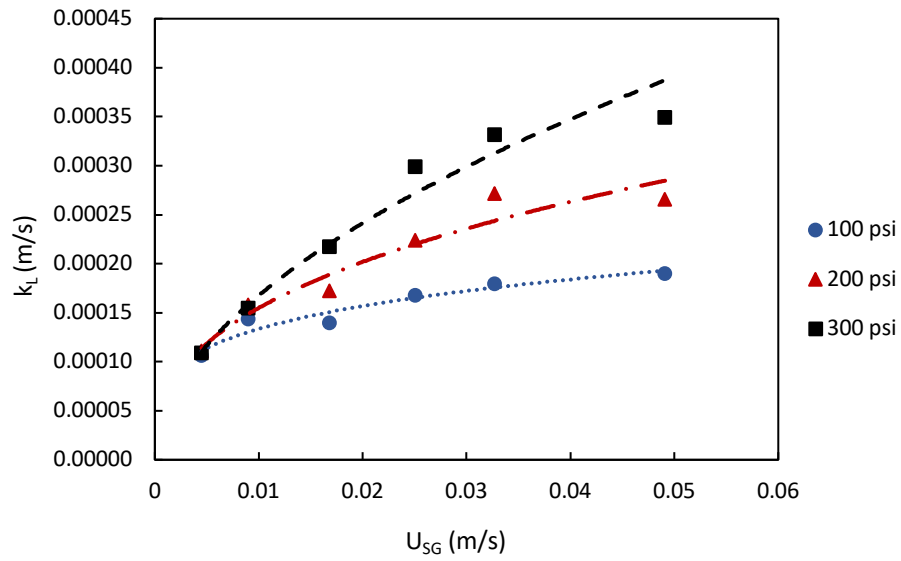
5.2. Image Analysis

5.2.1 Influence of Parameters on Mass Transfer Kinetics and Interfacial Area

Measurements of the volumetric mass transfer coefficient, the liquid-side mass transfer coefficient and interfacial area were calculated at various operating pressure (100, 200 and 300 psi) at superficial gas velocities ranging from 0.0045-0.0491 m/s. The values and the effect of the superficial gas velocity with increasing operating pressure are shown in Figure 5.2. The values of $k_L a$, k_L and a increase with an increase in superficial gas velocity as supported by many studies (Han et al. 2006; Jin et al. 2014; Sujan et al. 2017). The liquid-side mass transfer coefficient was calculated from the measured $k_L a$ and a values. The k_L values increased with the superficial gas velocity at low ranges of gas velocity. At higher superficial gas velocity ranges, the k_L values flatten out or change becomes small with further increases in gas velocity similarly to the results by Han et al. 2006. With an increase in superficial gas velocity there is an increase in turbulence leading to higher mass transfer rate. There is also an increase in interfacial area with increasing

superficial gas velocity because average bubble size decreases due to bubble breakup and the results shown in Figure 5.2(a) agree with previous studies. Even though there is a decrease in contact time between the methane and internal olefin at higher gas velocities, the increase in k_L and a are significant enough to lead to increasing values of $k_L a$.



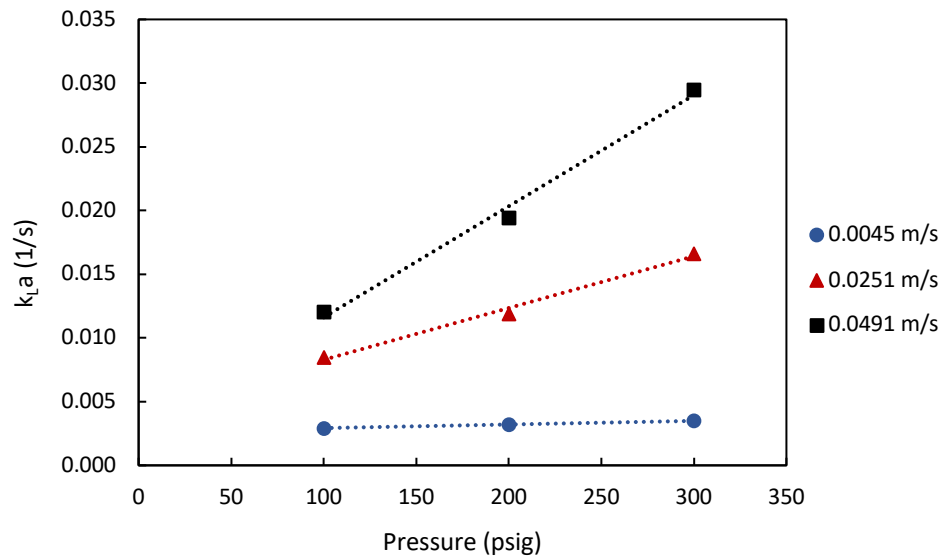


(c)

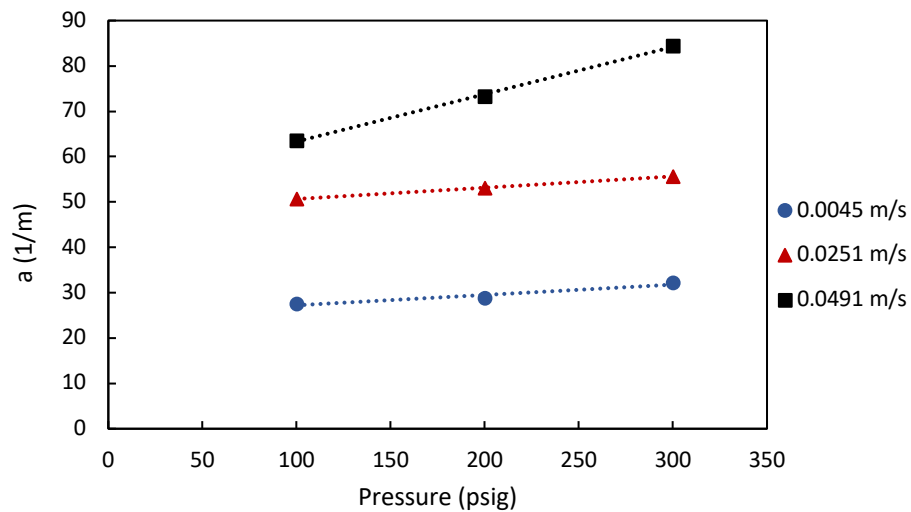
Figure 5.2. Image analysis results for the influence of superficial gas velocity on mass transfer kinetics and interfacial area. A: Influence of increased U_{SG} on $k_L a$. B: Influence of increased U_{SG} on interfacial area. C: Influence of increased U_{SG} on k_L .

The effect of operating pressure on $k_L a$, k_L and a were experimentally determined and the results are shown in Figure 5.3. The resulting values were determined for increasing pressures ranging from 100-300 psi at 3 different superficial gas velocities (0.0045, 0.0251 and 0.0491 m/s). Figure # shows that the $k_L a$, k_L and a values increase with pressure at higher ranges of superficial gas velocity. For the lowest superficial gas velocity, there is not a significant effect of operational pressure on the $k_L a$ values, but with increasing superficial gas velocity, operating pressure has a more significant influence. For the values of liquid-side mass transfer and interfacial area, there was also a more significant influence of operating pressure at higher superficial gas velocities which is shown in Figure 5.3(b-c). At higher operating pressures, there are more bubble breakups, and the ability of bubble coalescence is suppressed which leads to smaller bubble formation and an increase in interfacial area with increasing pressures. The increase in the liquid-side mass transfer coefficient at increasing pressures can likely be attributed to the change in liquid properties

like surface tension and viscosity (Han et al. 2006). Lower surface tension allows for formation of small gas bubbles in the liquid which results in the increase in interfacial area. The decrease in liquid viscosity is significant in allowing for better mass transfer due to a low resistance in the liquid film. The increase in operating pressure leads to the increase in k_L and a values and inevitably leads to an increase in $k_L a$ values, especially at higher superficial gas velocity ranges.



(a)



(b)

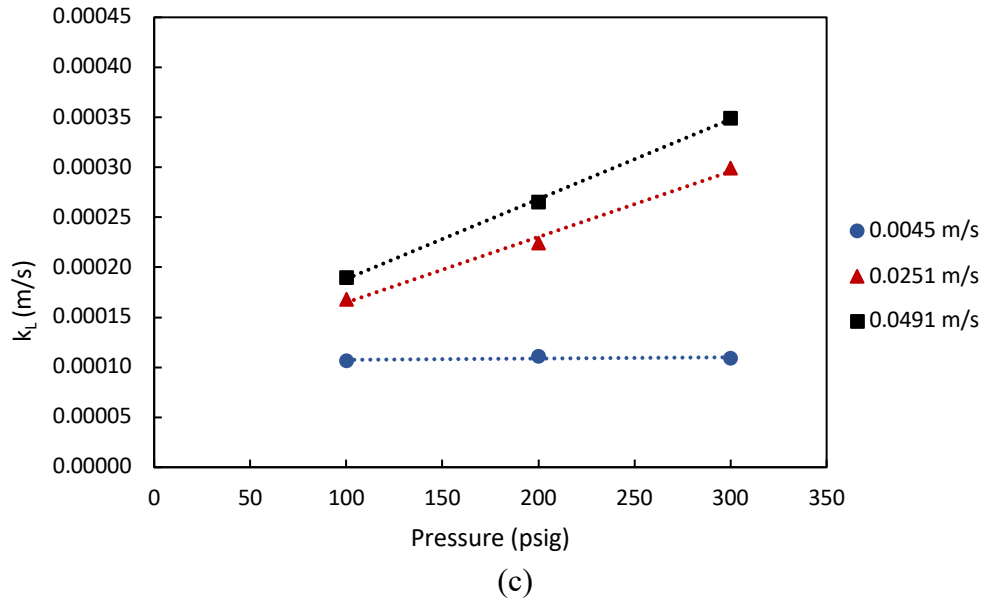


Figure 5.3. Image analysis results for the influence of operating pressure on mass transfer kinetics and interfacial area. A: Influence of increased pressure on $k_L a$. B: Influence of increased pressure on interfacial area. C: Influence of increased pressure on k_L .

5.2.2 Influence of Parameters on Gas Holdup

Measurements of overall gas holdup, ε_G , were calculated for different operating pressures (100, 200 and 300 psi) with increasing superficial gas velocity ranging from 0.0045-0.0491 m/s. The effect of superficial gas velocity and operating pressure on the overall gas holdup was determined and the results are shown in Figure 5.4. The overall gas holdup increased with both an increase in superficial gas velocity and slightly increased with an increase in operating pressures, as explained by many studies (Letzel et al. 1999; Lau et al. 2004; Han et al. 2006). As shown before, with an increase in superficial gas velocity there is a decrease in average bubble diameter but an increase in number of bubbles. This overall increase in interfacial area with increasing gas velocity and operating pressure can be explained primarily as a result of the higher overall gas holdup within the system.

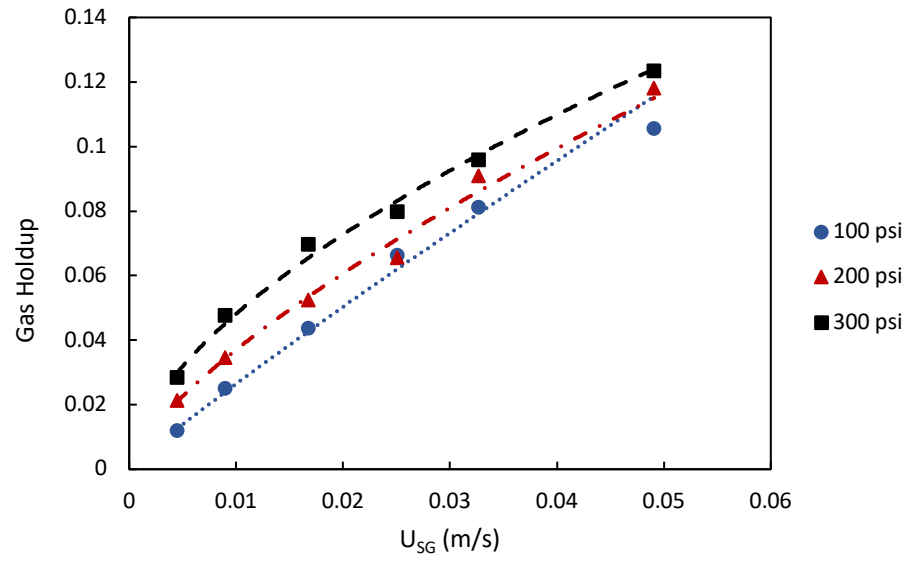


Figure 5.4. Influence of superficial gas velocity and operating pressure on gas holdup

Chapter 6. RECOMMENDATIONS AND CONCLUSION

By investigating the interaction between methane and non-aqueous fluids, the influence of several key parameters on the absorption mass transfer kinetics has been determined. This experimental study can bridge the gap between limited studies on the interaction of gas and non-aqueous fluids and the future work of developing a model to simulate the absorption process in different riser gas management scenarios. Through the development of the low and high pressure mass transfer experimental apparatus and procedures, the absorption process of methane into base fluids could be investigated under various experimental conditions. In this study, the effect of operating pressure (100-800 psi), superficial gas velocity (0.45-4.91 cm/s), fluid type (diesel and internal olefin), sparger design and column diameter (1.0-2.625 in.) on the volumetric absorption mass transfer coefficient was experimentally investigated. This study employed a low and high pressure apparatus to test various ranges of parameters and allow for experiments above 300 psi. During the experiments, the mass transfer coefficient ($k_L a$) value was determined for each experimental test based on the model presented by Álvarez et al. (2000). From the experimental study, the following conclusions were determined under these set experimental conditions shown:

- An increase in superficial gas velocity leads to an increase in the volumetric absorption mass transfer coefficient for methane in non-aqueous fluids. As superficial gas velocity increases it leads to more smaller bubbles due to bubble breakup and increases the interfacial area causing an increase in $k_L a$.
- An increase in operating pressure also leads to an increase in the $k_L a$ values. As superficial gas velocity increases, the effect of pressure on $k_L a$ becomes even more significant.
- Column dimensions and coarse bubble sparger designs did not influence the mass transfer kinetics in this experimental study.

- A high-speed camera and image analysis can be used to determine the interfacial area (a) of the absorption experiments, leading to the calculation of the liquid-side mass transfer coefficient (k_L) and gas holdup.
- Because of the significant influence of operating pressure and superficial gas velocity for this specific experimental setup, the $k_L a$ correlation was developed as a function of pressure and superficial gas velocity.
- In Appendix B, dimensionless analysis was performed to develop a dimensionless mass transfer correlation using the Stanton and Reynold's numbers.

The absorption experiments were conducted with non-aqueous base fluids, mostly using internal olefins. In a drilling process, the drilling fluids used can have several additives to the base fluids that was not investigated in this study. Future experimental work should include non-aqueous drilling fluids and investigate the effect of additives like emulsifier and viscosifier, as well as different oil to water emulsion ratios. The expansion of the investigation of methane in different drilling fluids could lead to direct value measurements needed for well control events. In making the experimental data more applicable to drilling scenarios, the additional tests of increased pressure and temperature ranges should also be investigated. Experiments at high pressure and temperature ranges for methane in non-aqueous base fluids should be conducted to determine the effect on absorption mass transfer kinetics under well control operating conditions. With further experimental investigations, the volumetric mass transfer coefficients, liquid-side mass transfer coefficients, interfacial area and gas holdup could be used in models for accurate simulations of well control events.

APPENDIX A. Experimental Data Used for the Calculation of $k_L a$

In Appendix A, the experimental data for the calculation of $k_L a$ for methane in internal olefins at 100 psi is shown as an example. This data was shown in Figures 3.4-3.6 in the volumetric mass transfer calculations sections. The data shown is from 4 experiments at various flow rates from 1-6 ln/min or superficial gas velocities ranging from 0.45-2.51 cm/s. The amount of methane (L) that is dissolved in the internal olefins at various time intervals throughout the duration of the experiment is shown which is then used to calculation the mols of gas and concentration of gas in solution. This data is directly used to calculate the $k_L a$ values for the 4 experimental tests.

Table A.1. Experimental data for absorption tests of methane in internal olefin at 100 psi and superficial gas velocities ranging from 0.45-2.51 cm/s

Trial	U_{SG} (cm/s)	Time (s)	Total Absorbed (L)	n (mol)	Concentration of Methane in IO (mol/L)	$\ln\left(\frac{C^*}{C^* - C_L}\right)$
-	-	0	0	0	0	0
1	0.45	30	0.2	0.008	0.016	0.140
2	0.45	60	0.4	0.017	0.033	0.303
3	0.45	120	0.6	0.025	0.049	0.497
4	0.45	300	1.0	0.041	0.082	1.060
5	0.45	600	1.3	0.054	0.107	1.894
6	0.45	900	1.4	0.058	0.115	2.465
7	0.45	1200	1.53	0.063	0.126	
Trial	U_{SG} (cm/s)	Time (s)	Total Absorbed (L)	n (mol)	Concentration of Methane in IO (mol/L)	$\ln\left(\frac{C^*}{C^* - C_L}\right)$
-	-	0	0	0	0	0
1	0.90	30	0.3	0.012	0.025	0.218
2	0.90	60	0.5	0.021	0.041	0.396
3	0.90	120	0.7	0.029	0.058	0.612
4	0.90	300	1.2	0.050	0.099	1.534
5	0.90	600	1.4	0.058	0.116	2.465
6	0.90	900	1.53	0.063	0.126	

(table cont'd.)

Trial	U_{SG} (cm/s)	Time (s)	Total Absorbed (L)	n (mol)	Concentration of Methane in IO (mol/L)	$\ln\left(\frac{C^*}{C^* - C_L}\right)$
-	-	0	0	0	0	0
1	1.68	30	0.5	0.021	0.041	0.396
2	1.68	60	0.7	0.029	0.058	0.612
3	1.68	120	1.1	0.045	0.091	1.269
4	1.68	300	1.4	0.058	0.116	2.465
5	1.68	600	1.5	0.062	0.124	3.932
6	1.68	900	1.53	0.063	0.126	
Trial	U_{SG} (cm/s)	Time (s)	Total Absorbed (L)	n (mol)	Concentration of Methane in IO (mol/L)	$\ln\left(\frac{C^*}{C^* - C_L}\right)$
-	-	0	0	0	0	0
1	2.51	30	0.6	0.025	0.050	0.470
2	2.51	60	1.1	0.045	0.091	1.163
3	2.51	120	1.5	0.062	0.124	2.773
4	2.51	300	1.53	0.066	0.132	

APPENDIX B. Development of Dimensionless Mass Transfer Correlation

When reporting values of mass transfer coefficients, it is more commonly reported as part of a correlation of dimensionless numbers (Cussler 2009). Two common dimensionless numbers that include the mass transfer coefficient term are Sherwood and Stanton numbers. Along with the two mass transfer dimensionless groups, there are dimensionless groups that describe different types of diffusion and flow within a system. Use of these dimensionless correlations give reasonable estimations of mass transfer coefficients without conducting experiments under each testing condition. Aeration is a common industrial process that allows for the use of Stanton number to adequately predict the mass transfer coefficient as follows:

$$ka = ka(v, \rho, \mu, d, z) \quad [B.1]$$

$$ka = [constant] v^\alpha \rho^\beta \mu^\gamma d^\delta z^\epsilon \quad [B.2]$$

Cussler (2009) shows that the mass transfer coefficient is a function of velocity (v), gas density (ρ) and viscosity (μ), diameter (d) and height (z) of the liquid. Deriving the equations, the following dimensionless correlation is developed:

$$\left(\frac{kad}{v}\right) = [constant] \left(\frac{dv\rho}{\mu}\right)^{-\gamma} \left(\frac{z}{d}\right)^\epsilon \quad [B.3]$$

$$\text{Stanton Number (St)} = \frac{kad}{v}$$

$$\text{Reynold's Number (Re)} = \frac{dv\rho}{\mu}$$

The developed correlation shows Stanton number (St) on the left-hand side of the equation, with the Reynold's number (Re) as the first term and tank's depth as the second term on the right-hand side. In the experimental design, the height and diameter of the column was constant resulting in the following correlation:

$$\left(\frac{kad}{v}\right) = [C] \left(\frac{dv\rho}{\mu}\right)^{-\gamma} \quad [\text{B.4}]$$

The developed correlation did not strongly correlate to the experimental data for all pressure conditions from 100-300 psi in the same correlation. As a result, the dimensionless correlation was developed for each pressure condition and shown in Table B.1:

Table B.1: Developed dimensionless mass transfer correlation for each pressure condition

<i>Pressure</i>	<i>C</i>	<i>γ</i>	<i>Equation</i>
100	0.01035	0.3951	$St = 0.01035 * (Re)^{0.3951}$
200	0.01558	0.2327	$St = 0.01558 * (Re)^{0.2327}$
300	0.01879	0.0874	$St = 0.01879 * (Re)^{0.0874}$

Following the development of the dimensionless mass transfer correlation for each pressure condition, a dimensionless pressure term was added to the correlation to develop 1 equation for all experimental conditions as follows:

$$\left(\frac{kad}{v}\right) = [C] \left(\frac{dv\rho}{\mu}\right)^{-\gamma} \left(\frac{P}{P_{atm}}\right)^{\epsilon} \quad [\text{B.5}]$$

The new term uses the experimental pressure (P) over atmospheric pressure (P_{atm}) to develop a dimensionless correlation with a pressure term. With the experimental data, the following correlation was developed:

$$St = 0.0126 (Re)^{-0.2016} \left(\frac{P}{P_{atm}}\right)^{0.428} \quad [\text{B.6}]$$

The variables considered in the dimensional analysis are parameters included in this study, but other parameters could be considered which would change the form of the dimensionless correlation to predict the mass transfer coefficient.

BIBLIOGRAPHY

- Ahmed, Fadha & Sensenich, Brent & Ghenni, Saba & Znerdstrovic, Daniel & Al-Dahhan, Muthanna. (2015). Bubble Dynamics in 2D Bubble Column: Comparison between High-Speed Camera Imaging Analysis and 4-Point Optical Probe. *Chemical Engineering Communications*. 202. 10.1080/00986445.2013.803076.
- Akita, Kiyomi, and Fumitake Yoshida. 1973. "Gas Holdup and Volumetric Mass Transfer Coefficient in Bubble Columns. Effects of Liquid Properties." *Industrial & Engineering Chemistry Process Design and Development* 12, no. 1 (1973): 76–80. <https://doi.org/10.1021/i260045a015>.
- Álvarez, E., B. Sanjurjo, A. Cancela, and J.m. Navaza. 2000. "Mass Transfer and Influence of Physical Properties of Solutions in a Bubble Column." *Chemical Engineering Research and Design* 78, no. 6 (2000): 889–93. <https://doi.org/10.1205/026387600527950>.
- Bensler, P. H. (1990). Ultrasonic determination of interfacial area, void fraction, and Sauter mean diameter in bubbly flow. Ph.D. thesis, Institute National Polytechnique de Grenoble, France.
- Besagni, G., Inzoli, F., Ziegenhein, T., 2018. Two-phase bubble columns: a comprehensive review. *Chem. Eng.* 2 (2), 13.
- Bourgoynne, Adam T., Scott, Stuart L., and James B. Regg. "Sustained Casing Pressure in Offshore Producing Wells." Paper presented at the Offshore Technology Conference, Houston, Texas, May 1999. doi: <https://doi.org/10.4043/11029-MS>
- Bradley, Nigel & Eric, Low & Aas, Bjarne & Rolv, Rommetveit & Larsen, Hans. (2002). Gas Diffusion - Its Impact on a Horizontal HPHT Well. 10.2523/77474-MS.
- Cussler, E. (2009). Fundamentals of Mass Transfer. In *Diffusion: Mass Transfer in Fluid Systems* (Cambridge Series in Chemical Engineering, pp. 237-273). Cambridge: Cambridge University Press. doi:10.1017/CBO9780511805134.010
- Deckwer, W. D., Burckhart, R. and Zoll, G., 1974, Mixing and mass transfer in tall bubbles, *Chem Eng Sci*, 29: 2177-2188. [https://doi.org/10.1016/0009-2509\(74\)80025-4](https://doi.org/10.1016/0009-2509(74)80025-4)
- Deshpande, Suraj & Kar, Kishore & Pressler, Jim & Tebeka, I. & Martins, B. & Rosenfeld, D. & Biggs, J.(2019). Mass Transfer Estimation for Bubble Column Scale Up. *Chemical Engineering Science*. 205. 10.1016/j.ces.2019.05.011.
- Feng, J., Fu, J., Chen, P., Du, Z., Qin, L. (2016). Experimental study and molecular simulation of gas dissolution and diffusion behavior in drilling fluid, *Journal of Natural Gas Science & Engineering*, doi: 10.1016/j.jngse.2016.10.060.

- Feng, Jian & Fu, Jianhong & Chen, Ping & Xu, Liqun. (2019). Investigation of methane/drilling mud phase behavior and its influence to hydrocarbon drilling activity. *Energy Science & Engineering*. 7. 10.1002/ese3.345.
- Flatabø, G.Ø.; Torsvik A.; Oltedal V.M.; Bjørkvik B.; Grimstad A-A.; Linga H. 2015. SPE-173865-MS. Experimental Gas Absorption in Petroleum Fluids at HPHT Conditions. SPE Bergen One Day Seminar held in Bergen, Norway, 22 April 2015
- Gandhi, Ankit B., Prashant P. Gupta, Jyeshtharaj B. Joshi, Valadi K. Jayaraman, and Bhaskar D. Kulkarni. 2009. "Development of Unified Correlations for Volumetric Mass-Transfer Coefficient and Effective Interfacial Area in Bubble Column Reactors for Various Gas-Liquid Systems Using Support Vector Regression." *Industrial & Engineering Chemistry Research* 48, no. 9 (June 2009): 4216–36. <https://doi.org/10.1021/ie8003489>.
- Han, Lu & Al-Dahhan, Muthanna. (2007). Gas-Liquid Mass Transfer in a High Pressure Bubble Column Reactor with Different Sparger Designs. *Chemical Engineering Science*. 62. 131-139. 10.1016/j.ces.2006.08.010.
- Hibiki, T., Ishii, M., & Xiao, Z. (2001a). Axial interfacial area transport of vertical bubbly flows. *International Journal of Heat and Mass Transfer*, 44, 1869–1888.
- Hikita, H., Asai, S. and Nose, H., 1974, Absorption of sulfur dioxide into water, *AIChEJ*, 24: 147-149.
- Hikita, H., Asai, S., Tanigawa, K., Segawa, K., Kitao, M., 1981. The volumetric liquid- phase mass transfer coefficient in bubble columns. *Chem. Eng. J.* 22 (1), 61–69.
- Jin, Haibo, Suohe Yang, Guangxiang He, Delin Liu, Zemin Tong, and Jianhua Zhu. 2014. "Gas-Liquid Mass Transfer Characteristics in a Gas-Liquid-Solid Bubble Column under Elevated Pressure and Temperature." *Chinese Journal of Chemical Engineering* 22, no. 9 (2014): 955–61. <https://doi.org/10.1016/j.cjche.2014.06.019>.
- Kiambi S. L., Duquenne A. M., Bascoul A. and Delmas H. (2001). "Measurements of local interfacial area: application of bi-optical fiber technique", *Chem Eng Sci*, 56: 6447-6453
- Koide, K.; Takazawa, A.; Komura, M.; Matsunaga, H. Gas holdup and volumetric liquid-phase mass transfer coefficient in solid-suspended bubble columns. *J. Chem. Eng. Jpn.* 1984, 17, 459–466.
- Lackey, G., & Rajaram, H. (2019). Modeling gas migration, sustained casing pressure, and surface casing vent flow in onshore oil and gas wells. *Water Resources Research*, 55, 298–323. <https://doi.org/10.1029/2018WR024066>
- Lau, R., W. Peng, L. G. Velazquez-Vargas, G. Q. Yang, and L.-S. Fan. 2004. "Gas-Liquid Mass Transfer in High-Pressure Bubble Columns." *Industrial & Engineering Chemistry Research* 43, no. 5 (2004): 1302–11. <https://doi.org/10.1021/ie030416w>.

- Linga, H., Torsvik, A. and Saasen A., 2016. Kick Detection Capability of Oil-based Muds in Well Control Situations. SPE-180039-MS, presented at the SPE Bergen One Day Seminar, Bergen, Norway 20 April 2016.
- Linga, Harald & Bjoerkevoll, Knut Steinar & Skogestad, Jan Ole & Saasen, Arild. (2017). Gas Influx into Drilling Fluids During Flow Check Operations as Affected by Gas Absorption Characteristics of the Drilling Fluid. 10.2118/184686-MS.
- H.M. Letzel; J.C. Schouten; R. Krishna; C.M. van den Bleek (1999). Gas holdup and mass transfer in bubble column reactors operated at elevated pressure. *54(13-14)*, 2237–2246. doi:10.1016/s0009-2509(98)00418-7
- Malloy, Kenneth P., Rick Stone, George Harold Medley, Don M. Hannegan, Oliver D. Coker, Don Reitsma, Helio Mauricio Santos, et al. 2009. “Managed-Pressure Drilling: What It Is and What It Is Not.” IADC/SPE Managed Pressure Drilling and Underbalanced Operations Conference & Exhibition, 2009. <https://doi.org/10.2118/122281-ms>.
- Neff, Jerry M., S. McKelvie, and R. C. Ayers. 2000. Environmental Impacts of Synthetic Based Drilling Fluids. New Orleans: U.S. Dept. of the Interior, Minerals Management Service, Gulf of Mexico OCS Region, 2000.
- O'bryan, Patrick Leon, "Well Control Problems Associated with Gas Solubility in Oil-Based Drilling Fluids." (1988). LSU Historical Dissertations and Theses. 4524.
- Ribeiro, Paulo & Pessôa Filho, Pedro & Lomba, Rosana & Bonet, Euclides. (2006). Measurement and modeling of methane dissolution in synthetic liquids applied to drilling fluid formulation for deep and ultradeep water wells. *Journal of Petroleum Science and Engineering*. 51. 37-44. 10.1016/j.petrol.2005.11.007.
- Sada, E., Kumazawa, H, Lee, C.H., & Narukawa, H. (1987). Gas–liquid interfacial area and liquid-side mass-transfer coefficient in a slurry bubble column. *Industrial and Engineering Chemistry Research*, 26, 112–116.
- Shah, Y.T.; Kelkar, B.G.; Godbole, S.P.; Deckwer, W.D. Design parameters estimations for bubble column reactors. *AIChE J.* 1982, 28, 353–379.
- Silva, C. T., Mariolani, J. R. L., Bonet, E. J., Lomba, R. F. T., Santos, O. L. A., Ribeiro, P. R., 2004. Gas solubility in synthetic fluids: a well control issue. In SPE Annual Technical Conference and Exhibition. Society of Petroleum Engineers.
- Skogestad, J.O., Linga, H., Bjørkevoll K.S. and Saasen A., 2017. Methodology for Predicting Gas Loading Capability in Oil-based Drilling Fluids. SPE-184710-MS, SPE/IADC Drilling Conference and Exhibition, The Hague, The Netherlands, March 2017.
- Sujan, Ajay & Vyas, Raj & Singh, Kailash. (2018). Estimation of liquid-side mass transfer coefficient and liquid film thickness in a bubble column using single spherical bubble model. *Asia-Pacific Journal of Chemical Engineering*. 13. 10.1002/apj.2178.

- Wilkinson, Peter M., Herman Haringa, and Laurent L. Van Dierendonck. 1994. "Mass Transfer and Bubble Size in a Bubble Column under Pressure." *Chemical Engineering Science* 49, no. 9 (1994): 1417–27. [https://doi.org/10.1016/0009-2509\(93\)e0022-5](https://doi.org/10.1016/0009-2509(93)e0022-5).
- Wilkinson, P.; Speck, A.; van Dierendonck, L., 1992. Design parameters estimation for scale-up of high-pressure bubble columns. *AIChE J.* 38 (4).
- Xu, Rong, "Analysis of diagnostic testing of sustained casing pressure in wells" (2002). LSU Doctoral Dissertations. 1192.
https://digitalcommons.lsu.edu/gradschool_dissertations/1192
- Xue J. Bubble Velocity, Size and Interfacial Area Measurement in Bubble Columns. PhD dissertation. St. Louis: Washington University, 2004.
- Yun, B. J. (1996). Measurement of two-phase flow parameters in the subcooled boiling. Ph.D. thesis, Seoul National University, Korea.

VITA

Scott A. Perry is from Van Buren, Arkansas. He received his bachelor's degree in Chemical Engineering from the University of Arkansas in May 2019. In June 2019, he began his education at Louisiana State University to earn a Master of Science degree in the Craft and Hawkins Department of Petroleum Engineering. Scott is planning on earning his degree in August 2021. During his undergraduate and graduate studies, he had the opportunity to work for ExxonMobil and FutureFuel Chemical Company as an operations and chemical engineering intern respectively. Scott has accepted a second internship with ExxonMobil in the Global Projects group as a Process Design Engineer for summer 2021 before his graduation from Louisiana State University.